Yugoslav Journal of Operations Research
(20##), Number #, #-#
DOI: https://doi.org/10.2298/YJOR240315018K

EMENDED SNAKE OPTIMIZER TO SOLVE MULTIOBJECTIVE HYBRID ENERGY GENERATION SCHEDULIN G

Avneet KAUR

Department of Electrical and Instrumentation Engineering, Sant Longowal Institute of Engineering and Technology
avneetdhaliwal2@gmail.com

J.S. DHILLON

Department of Electrical and Instrumentation Engineering, Sant Longowal Institute of Engineering and Technology
jsdhillonp@yahoo.com

Manmohan SINGH

Department of Electrical and Instrumentation Engineering, Sant Longowal Institute of Engineering and Technology
singh_manmohan@msn.com

Received: March 2024 / Accepted: May 2024

Abstract: This paper proposes an emended snake optimizer (ESO) for solving hydrothermal, pumped hydro, and solar generators' non-convex, highly constrained, and non-linear power generation scheduling problem. The generation scheduling problem aims to reduce thermal generator operating costs and pollutants by maximizing hydro volume and utilizing solar power generation. The minimization of operating costs and pollutants is subjected to various constraints, like meeting load demand, active power generation violations, water volume utilization, etc. The conflicting objectives of the multiobjective generation scheduling are handled using the non-interactive approach exploiting the price-penalty method. The direct heuristics search is utilized to satisfy the load demand and water volume constraints. The snake optimization algorithm (SOA) often gets stuck in the local minima while solving complex engineering optimization problems, resulting in sluggish convergence behavior. The basic SOA is emended through simple search and opposition-based learning, enhancing exploitation, convergence behavior, and procuring near to global solutions. The simulation studies involve solving unconstrained standard benchmark problems and electric power system problems. The proposed emended snake optimizer offers significant cost savings for electric power systems ranging from 10-15%. Statistical

analysis using Wilcoxon signed-rank test and Friedman's test justifies the amendment. The rapid convergence behavior and Whisker box plots justify the proposed ESO's robustness.

Keywords*:* Coordinated generation scheduling, renewable energy, Snake optimization algorithm, simplex search method, opposition-based learning, metaheuristics optimization, Optimization problem.

1. INTRODUCTION

Worldwide, growing electric power consumption and rapid inflation in fuel costs need the search for a novel power source for a generation. The electric power network should include a variety of energy sources. These are commonly referred to as non-conventional energy sources. Solar energy has been identified as the most promising non-conventional source of electricity generation in the future [1]. The key renewable energy source that is also storable is hydropower. This energy resource contributes significantly to the global production of renewable energy-generated electricity. Researchers are increasingly interested in non-traditional sources. The public's growing awareness of environmental difficulties generated by conventional power generation methods lends credence to non-conventional power generation alternatives [2]. Renewable energy sources and thermal generating units are considered in the coordinated problem to meet the area's generation requirement. Environmental considerations must also be addressed when using thermal units to generate electricity. As a result, the problem becomes a multi-objective coordinated economic generation scheduling problem with two objectives to minimize concurrently, namely the fuel cost of thermal units and pollutant emissions during coal burning. Both goals are inherently antagonistic. Hydro and solar energy sources help to cut thermal power generation costs while lowering pollutant emissions due to the reduced use of coal. These resources have the potential to lower the risk of electrical power generation. As a result, proper management of these sources is required for both economic and reliability reasons.

Pumped-storage plants and conventional plants are the two different categories of hydropower plants. Traditional plants may also be run-of-river plants or storage plants. Run-of-river plants don't store much water and only use it when it's needed. When water is wasted, spills happen. Water reservoirs in storage-type plants have a certain amount of storage space. Scheduling issues for hydrothermal generating can be divided into long-term and short-term. The scheduling horizon for long-term planning is one year, whereas the horizon for short-term planning is either one day or one week. A fixed-head hydrothermal generation scheduling problem exists when a hydroelectric power plant has a reservoir with a large capacity, and the head of the reservoir is expected to be stationary. The hydrothermal scheduling problem is known as variable-head hydrothermal scheduling if the hydropower plants have reservoirs with a low capacity [3]. The primary function of a pumped storage hydroelectric (PSH) power station is to store cost-effective extra electrical power that becomes available during off-peak load periods when water energy stored is satisfied by pumping water from the lower storage reservoir to the top storage reservoir. The water potential energy stored is utilized to produce electricity when demand is high [4]. In order to address the water issue and guarantee optimal water utilization, a PSH unit can also be created with hydroelectric plants [5, 6].

Furthermore, because of the availability of water and solar radiation variability, the entire power demand is not put on renewable energy sources. Thermal generating units

help renewable energy sources continue offering consumers electrical power. As a result, to account for the uncertainties of the sun, the overall participation is restricted by the spinning reserves maintained by thermal units. The unit commitment assures that the solar generation share does not exceed the authorized power share [7]. The benefit of securing a fixed percentage of electricity demand from solar units is that it provides an uninterrupted power supply. As a result, retaining thermal-producing units in the system is required. The impacts of incorporating solar energy are simulated, and the spinning reserve required is factored into the inequality constraint. Generation scheduling is primarily a non-linear, multi-objective, multivariable, and highly constrained optimization problem. Other renewable solid and liquid fuels, such as biomass, hydrogen fuel, and biodiesel fuels, can play an important role in the primary energy supply and the economy in the future due to their storability [8] because solar and thermal unit scheduling can result in significant financial savings [9]. Hybrid energy generation scheduling (HEGS) is defined as combining generations from thermal, hydro, pumped storage, and solar units [10]. Despite being clean and green, renewable energy sources are not isolated due to their low ability to provide electricity. For more cost-effective operation, a hybrid power system combines conventional and renewable energy sources, such as thermal-solar photovoltaic power plants [11, 12], thermal power units [13], pumped storage hydro-solar units [14], etc. The production of hybrid energy systems has also been corrected in another effort [15]. The development of materials and their characterization is very important field for the development of photovoltaic solar cells. Dahmani et al. [16] provided valuable insights into tailoring the properties of Ti-25Nb-25 Mo alloy through controlled milling processes for specific applications, especially in the biomedical field. Zulqarnain et al. [17] addressed both theoretical advancements in statistical measures for interval-valued intuitionistic fuzzy hyper soft set information and practical implications in decision-making and system optimization, particularly in thermal energy storage. Ullah et al. [18] combined theoretical modeling, numerical analysis, and practical implications, making it relevant for understanding complex fluid behaviors and their applications in engineering systems, particularly in heat transfer and cooling processes.

The problem of generation scheduling can be solved using a variety of optimization methods [19, 20], including dynamic programming [21], neural networks [22], simulated annealing [23], evolutionary programming [24], Harris hawks optimizer [25], genetic algorithm [26], multi-objective genetic algorithm [27], Lagrangian relaxation [28-30], branch and bound algorithm [31], Tabu search [32], and particle swarm optimization [33]. When solar sources are considered, forecasting makes the generation scheduling problem uncertain. Numerous studies have examined the issue of generation scheduling with solar cost. [34-40].

Nguyen et al. [41] developed an adaptive selective cuckoo search method to handle short-term hydrothermal scheduling problems. Logarithmic mixed-integer linear programming was used by Jian et al. [42] to handle short-term hydrothermal scheduling problems. Yin et al. [43] employed crisscross optimization to fix problems with short-term hydrothermal generation scheduling. The hydrothermal generating scheduling with pumped storage and solar units is recommended to use the TVAC-PSO integrated optimization approach, as described by Patwal et al. [44]. Kaur et al. [45] employed a crisscross differential evolution method to handle hydrothermal scheduling problems. Patwal and Narang [46] have provided a crisscross PSO-based solution to the scheduling of pumped storage hydrothermal generating and examined the effects of renewable sources

on cost and pollution emission. Ferreira [47] addressed the short-term pumped storage scheduling problem, and the author used the dynamic programming method to tackle restrictions. The evolutionary particle swarm optimization (EPSO) that Chen [48] introduced combines a fundamental PSO with binary encoding/decoding methods and a mutation operation. Binary encoding/decoding techniques are used to model the various aspects of a pumped storage system.

According to the literature review, the coordinated pumped-storage hydro-solar-thermal generation scheduling problem while considering environmental factors is barely implemented. In other words, if the coordinated generation scheduling problem has been resolved, either the influence of tilt angle in the solar model has not been considered, or the environmental effects of pollutants have been disregarded. Therefore, it is necessary to give a model that is similar to the real-time model. This work considers pumped-storage hydro and solar generating units in a multi-objective framework to address the HEGS problem and presents a hybrid technique to handle the problem.

Metaheuristic algorithms commonly incorporate random search techniques from nature. Most metaheuristic algorithms, as opposed to evolutionary algorithms, use genetic rules, such as information sharing, the strengthening of traits, and the survival of the fittest. Despite the similarities among these optimizers, nature-inspired optimizers have unique traits that set them apart regarding their search methodology. Hashim et al. [49] introduced the metaheuristic snake optimization algorithm (SOA) to solve global optimization, which takes inspiration from nature. The SOA is modelled on the mating of snakes. If enough food is available and the temperature is low, each snake competes to mate with the best female. Authors frequently use the SOA to summarize these commonalities since it has a strong balance between exploration and exploitation and a steady and rapid convergence rate. Numerous engineering problems have used SOA, including feature selection, quantum physics, and the medical industry. A snake optimizer was employed by Klimov et al. [50] to manage the settings of a quantum processor. Snake optimizer has improved the frequencies at which frequency-tunable superconducting qubits implement quantum logic circuits. For feature selection problems, Khurma et al. [51] presented a binary snake optimizer. The suggested approach is evaluated using the COVID-19 real data set and industry-standard benchmark functions. Al-Shourbaji et al. [52] presented the snake optimizer, a reptile search algorithm, to find the ideal feature offset. A significant preprocessing step, feature selection, aims to improve machine learning model performance while decreasing computational costs.

Heuristic methods are problem-solving techniques that use randomness. Therefore, sometimes, these methods stagnate in the local optima. The "stagnation" here refers to a situation where the algorithm gets stuck without making progress, leading to inefficient outcomes. This stagnation can happen for various reasons, such as inadequate search space exploration or being trapped in local optima (suboptimal solutions). When an algorithm stagnates, it can produce "inaccurate results" that don't accurately reflect the problem's true solution. Additionally, the time taken to converge or reach a near-to-global solution increases significantly, making the algorithm less efficient and practical, especially for complex optimization problems. To address these limitations of the original Snake Optimization Algorithm (SOA), amendments are proposed. One such amendment is incorporating a simplex search method. A simplex search is a type of optimization technique that explores the search space efficiently. The algorithm can improve its exploration capability by combining simplex search with SOA. Another amendment to

overcome the inefficiency of SOA is opposition-based learning. Opposition-based learning helps to diversify the search process and prevents the algorithm from being stuck in local minima (suboptimal solutions that are not globally optimal). A global solution in optimization refers to the best possible solution within the entire feasible solution space of a problem. In other words, the solution optimizes the objective function to its global minimum (in minimization problems) or global maximum (in maximization problems) across all possible valid solutions.

A new algorithm called the Emended Snake Optimizer (ESO) is proposed by integrating simplex search and opposition-based learning into the SOA. ESO aims to strike a balance between exploration (searching widely for potential solutions) and exploitation (focusing on known good solutions) while reducing the risk of getting trapped in suboptimal solutions. The possibility of an emended algorithm that performs better than any of its component algorithms alone inspired the idea of hybridizing an existing algorithm. The problem can be solved with more significant input and better outcomes in less time by improving the basic algorithm. Additionally, using hybrid methodologies improves exploration and exploitation and spotlights a variety of methods for achieving solution accuracy. Hybrid algorithms ensure better solutions, but that comes at the expense of increased algorithm complexity and the accumulation of a wider variety of control parameters. The local simplex search strategy, which prevents local stagnation and sluggish convergence and ultimately enhances the outcomes and convergence of basic SOA, is hybridized to strengthen SOA. The proposed ESO is found to be efficient in terms of exploration-exploitation balance and convergence curve speed. The paper's contribution is described below:

This work incorporates pumped storage hydro and solar generating units in a multi-objective framework to address the HEGS problem and presents a new technique to search for a global solution. The contribution of the paper is outlined below:

- A nature-inspired metaheuristic emended snake optimizer (ESO) is proposed to solve a non-linear and constrained multi-objective hybrid energy generation scheduling (HEGS) problem. The thermal, hydro, pumped storage hydro and solar units are considered for generation scheduling to meet the load demand requirements.
- By limiting the solar share to demand and keeping a spinning reserve, which is backup power capacity ready to be deployed when needed, the grid can ensure reliability even when solar generation fluctuates. Solar power units are committed to restrict the solar share to certain demand limits using optimistic one-point crossover method.
- The basic snake optimizer is amended with a simplex search technique and opposition-based learning to overcome its premature convergence and stagnating to a local solution.
- The direct heuristics based on proportional sharing handle load demand and allocated water volume constraints of constrained optimization problems.
- A non-interactive approach exploiting the price-penalty method is applied to solve the conflicting objectives of the multiobjective generation scheduling problem.
- Unconstrained (unimodal and multimodal) standard benchmark optimization problems and two hydrothermal electric power test systems are used to verify the efficacy of the proposed algorithm.

- The statistical significance of the proposed algorithm is conducted to ensure the robustness of the proposed algorithm by performing Friedman's test and the Wilcoxon sign rank test.

The remaining part of the paper is divided into seven sections. The mathematical description of the multi-objective hybrid energy generation scheduling (HEGS) problem is presented in Section 2. Section 3 discusses the commitment of solar units and the procedure to get the commitment table. Constraints on equality and inequality. Section 4 describes the procedure to get a feasible solution by handling the equality and inequality constraints. Section 5 discusses the ESO principles and the idea of combining simplex search and opposition-based learning with the snake optimization algorithm. Section 6 describes the proposed ESO's results and analyses its performance using twenty-five standard benchmark optimization problems, two electric power test systems, and a list of parameters and their tuning for the ESO. The significance of statistical findings is explained in this section. Section 7 offers the findings' conclusion.

2. HYBRID ENERGY GENERATION SCHEDULING PROBLEM

An electric grid is built using n_t thermal power generators, n_h hydropower generators, n_p pumped storage generators and n_s number of solar units. Short-term hydrothermal generation activities are scheduled for 24 hours or a day.

Objectives-

- To schedule the thermal, hydro, pumped-storage hydro, and solar generations for 24 hours (1 day) in order to reduce operating costs of thermal and solar power generations by utilizing the available water volume to its fullest extent.
- The generated hydrothermal and solar power schedule must satisfy each hydroelectric and pumped storage hydro unit's pre-specified reservoir volume and power load demand.
- Solar power share is restricted to certain demand limits to maintain the uninterrupted supply by committing the solar units using optimistic one-point crossover method.
- While minimizing the operating cost, the load demand is needed to attain energy balance and satisfy the water volume constraints of hydro and pumped storage hydro units.

2.1. Thermal model

The goal is to reduce the cost of fuel for the thermal generating units over the planning period. The quadratic equation typically yields the following results in determining the generator running cost [53]:

$$F^C(P_t) = \sum_{t=1}^{T}\left(\sum_{i=1}^{N_t} t_t(a_i + b_i P_{ti} + c_i P_{ti}^2 + |d_i sin(e_i(P_i^L - P_{ti}))|)\right) \quad (\$) \qquad (1)$$

where, $P_t = \left[P_{t1}, \dots, P_{t,n_t}\right]^T$ and $a_i, b_i, c_i, d_i \; and \; e_i$ are cost coefficients of i^{th} generator having units (\$/h), (\$/MWh), $(\$/MW^2h)$, $(\$/h)$, and (rad/MW), respectively. N_t represents the total number of thermal units.

The usage of coal as a traditional energy source makes it important to take the environment into account. Both the thermal operating cost and the number of gaseous

pollutants released into the atmosphere by coal combustion during electricity production are reduced [53].

Minimum emission of gaseous pollutants

$$F^E(P_t) = \sum_{t=1}^{T}\left(\sum_{i=1}^{N_t} t_t\left(a_{2i} + b_{2i}P_{ti} + c_{2i}P_{ti}^2 + d_{2i}exp(e_{2i}P_{ti})\right)\right) \quad \text{(Ton)} \tag{2}$$

A non-interactive approach that exploits the price penalty method is used to solve the conflicting objectives of the emission-constrained economic load dispatch problem. Considering environmental effects and power generation from conventional sources, the objective leading to pollutants' emission is unified with operating cost thermal units using the price penalty factor, as both objectives are quadratic. The unified operating cost objective function is rewritten as [54]:

$$F^{CE}(P_t) = \sum_{t=1}^{T}\left(F^C(P_t) + h\,F^E(P_t)\right) \tag{3}$$

where 'h' (price penalty factor) is described as the proportion of operating cost to the emission of pollutants of thermal units calculated at maximum thermal generator power outputs and is computed as:

$$h = \frac{\sum_{i=1}^{N_t}\left(a_i + b_iP_i^U + c_i\left(P_i^U\right)^2 + \left|d_i sin\left(e_i(P_i^L - P_i^U)\right)\right|\right)}{\sum_{i=1}^{N_t}\left(a_{2i} + b_{2i}P_i^U + c_{2i}\left(P_i^U\right)^2 + d_{2i}exp\left(e_{2i}P_i^U\right)\right)} (\$/Ton) \tag{4}$$

The characteristic equation is validated within the output power limits of thermal generation as

$$P_{ti} = \begin{cases} P_{ti} & ;(P_i^L \le P_{ti} \le P_i^U) \\ P_i^L & ;(P_{ti} < P_n^L) \\ P_i^U & ;(P_{ti} > P_i^U) \end{cases} \qquad (i \in [1, N_t]; t \in [1, T]) \tag{5}$$

2.2. Hydro model

In short-term hydrothermal scheduling issues, the hydro units operate for a small fuel cost, but the available water volume must be used to the utmost. As a result, the total discharge of the hydro units over the planning period must match the reservoir's predetermined water volume, which is as follows [55]:

$$\sum_{t=1}^{T} t_t\, q_{tj} = V_j \qquad (j \in [1, N_h]) \tag{6}$$

where N_h represents the total number of hydro units.

The input-output characteristics of a hydro generator are the variation in water discharge as a function of power output, $P_{km}$and net head, w_{kj}^hrespectively. The Glimn-Kirchmayer model [56] calculates the j[th] hydro unit's discharge rate (q_{tj}) for the t[th] sub interval as follows:

$$q_{tj} = K_j\, \emptyset\,(P_{tm})\Psi\left(w_{tj}^h\right) \qquad (j \in [1, N_h]; t \in [1, T]; m = j + N_t) \tag{7}$$

where K_j is the proportional constant, $\emptyset\left(P_{tj}\right)$and $\Psi\left(w_{tj}^h\right)$ are hydro-generation and reservoir water head functions, respectively, and are defined as:

$$\emptyset\,(P_{tm}) = x_jP_{tm}^2 + y_jP_{tm} + z_j \qquad (j \in [1, N_h]; t \in [1, T]; m = j + N_t) \tag{8}$$

$$\Psi\left(w_{tj}^{h}\right) = \alpha_j\left(w_{tj}^{h}\right)^2 + \beta_j w_{tj}^{h} + \gamma_j \qquad (j \in [1, N_h]; t \in [1, T]) \tag{9}$$

where x_j (m^3/MW^2h), y_j (m^3/MWh) and $z_j(m^3/h)$ are water discharge coefficients of the j^{th} hydro unit, $\alpha_j(m^{-2})$, $\beta_j(m^{-1})$and γ_j(unitless) are head variation coefficients of the j^{th} hydro unit

The reservoir of the j^{th} hydro unit is assumed to have vertical sides and a finite capacity to compute the effective head. Spillage only occurs when the reservoir's storage capacity is exceeded. The equation for effective head continuity is as follows:

$$w_{tj+1}^{h} = w_{tj}^{h} + \frac{t_t}{SA_j}\left(I_{tj} - q_{tj}\right) \quad (j \in [1, N_h]; t \in [1, T]) \tag{10}$$

where w_{tj}^{h} (m),t_t(h), $SA_j(m^2)$ and I_{tj} (m^3/h) representing the effective head, time interval, surface area of the reservoir, and the water inflow, respectively.

The output power limits on hydro units are imposed as

$$P_{ti} = \begin{cases} P_{ti}, & ;(P_i^L \le P_{ti} \le P_i^U) \\ P_i^L, & ;(P_{ti} < P_i^L) \\ P_i^U, & ;(P_{ti} > P_i^U) \end{cases} \qquad (i \in [N_t + 1, N_t + N_h]; t \in [1, T]) \tag{11}$$

2.3. Pumped storage model

During the peak load period, a pumped storage plant performs the same functions as a conventional plant. During peak load times, water from the higher reservoir is used as usual to power the turbines. During the low load phase, water from the lower reservoir is pumped into the upper reservoir to be accessible for use during the upcoming cycle of the peak load period. The generator switches to synchronous motor action at this time, driving the turbine, which is now acting as a pump. There are two operational modes for pumped storage systems: generating mode and pumping mode. When water volume declines during generation, the major goal is to keep it constant through pumping [57].

$$V_l^I = V_l^F - \left(\sum_{t=1}^{T} t_t q_{tl}^{+} - \sum_{t=1}^{T} t_t |q_{tl}^{-}|\right) \quad \left(l \in [1, N_p]; t \in [1, T]\right) \tag{12}$$

where, N_p represents the total number of pumped storage units. The pumping and generation modes are selected based on the load demand. During the generation mode (σ_G), the discharge of the pumped storage unit is given as:

$$q_{tl}^{+} = \chi_l^{+}|P_{tm}^2| + \xi_l^{+}|P_{tm}| + \varphi_l^{+} \quad \left(l \in [1, N_p]; m = N_t + N_h + l; t \in [1, T]\right) \tag{13}$$

During the pumping mode (σ_P), the discharge of the pumped storage unit is given as:

$$q_{tl}^{-} = \chi_l^{-}|P_{tm}^2| + \xi_l^{-}|P_{tm}| + \varphi_l^{-} \quad \left(l \in [1, N_p]; m = N_t + N_h + l; t \in [1, T]\right) \tag{14}$$

where χ_l^{+}, χ_l^{-} (m^3/MW^2h), ξ_l^{+}, ξ_l^{-} (m^3/MWh) and $\varphi_l^{+}, \varphi_l^{-}(m^3/h)$ are the coefficients of generation and pumping modes, respectively.

The power generation on pumped storage units should remain within limits, as given below.

$$P_{tl} = \begin{cases} P_{tl}, & ;(P_l^L \le P_{tl} \le P_l^U) \\ P_l^L, & ;(P_{tl} < P_l^L) \\ P_l^U, & ;(P_{tl} > P_l^U) \end{cases} \quad \left(l \in \left[N_t + N_h + 1, N_t + N_h + N_p\right]; t \in [1, T]\right) \tag{15}$$

2.4. Solar model

Solar energy is an eco-friendly form of generation. Solar energy is the energy that is created from solar radiation. The solar cell's output is of DC nature. Therefore, it must be converted into AC before moving it to the grids. A DC-to-AC converter is used to convert DC power into AC power. The AC power output is taken into account during optimal integration. A solar PV generator's overall cost follows a linear power generation function. The price of producing solar power is provided as [58]:

$$F(P_t^S) = \sum_{n=1}^{N_s} (C_N^S P_{tn}^S)\ (\$/h) \qquad (t \in [1, T]) \tag{16}$$

with $P_t^S = \left[P_{t1}^S, P_{t2}^S, \ldots, P_{tk}^S, \ldots, P_{t,}^S\right]^T$ and C_n^S $(\$/MWh)$is the cost coefficient of nth solar PV unit. N_s represents the total number of solar units.

The power generation from nth solar PV plant at the time, t is expressed as:

$$P_{tn}^S = I_{tn}^T A \eta_e \eta_d \eta_c \eta_w \tag{17}$$

where, P_{tn}^S is the output power (W), I_{tn}^T is the total solar radiation on the tilted PV array-hourly (W/m^2), A is the surface area of the PV array (m^2), η_e is an efficiency of PV array, η_d is a factor of degradation of the PV array, η_c is the efficiency of the power conditioning devices and η_w is the PV array wiring efficiency [57].

2.5. Coordinated hydrothermal-pumped storage-solar generation scheduling problem.

The aim is to keep the overall cost of operating thermal and solar units over the scheduling horizon (T) as low as possible. The capital cost of solar units is fixed. The equation for operating costs that must be minimized is as follows:

$$F(P_t, P_t^S) = \sum_{t=1}^{T} \left(F_i^{CE}(P_{ti}) + F_k(P_t^S)\right) \tag{18}$$

Subject to:

(i) Energy Balance equation: Along with the transmission losses of the power network, the combined power generation from all thermal, hydro, pumped storage, and solar generating units must meet the entire power demand [53].

$$\sum_{i=1}^{N_t} P_{ti} + \sum_{j=1}^{N_h} P_{tj} + \sum_{l=1}^{N_p} P_{tl} + \sum_{n=1}^{N_s} P_{tn} = P_{Dt} + P_{Lt} \qquad (t \in [1, T]) \tag{19}$$

whereP_{Dt} (MW) is total load demand and P_{Lt} (MW) represents the transmission losses and are calculated using Kron's loss formula as follows:

$$P_{Lt} = B_{00} + \sum_{i=1}^{N_g} B_{0i} P_{ti} + \sum_{j=1}^{N_g} \sum_{i=1}^{N_g} P_{ti} B_{ij} P_{ti}\ (t \in [1, T]) \tag{20}$$

with $N_g = N_t + N_h + N_p + N_s$

where B_{00} (MW), B_{0i}, $B_{ij}(MW^{-1})$ represents the loss coefficients evaluated by performing a.c., load flow analysis [53].

(ii) Solar power generation uncertainty

To prevent the system from deteriorating into a power shortage brought on by the unreliability of solar output, the entire demand cannot be placed on solar generators. As a result, solar energy production should account for no more than λ of the overall power consumption. Thermal power plants provide a base load, while solar energy provides a peak load. The permitted percentages of wind power [58]:

$$\sum_{n=1}^{N_S} P_{tn}^{S} \leq \lambda P_{Dt} \qquad (t \in [1,T]) \tag{21}$$

where λ is a constant, and its value is 0.3.

(iii) The water volume of hydro units

The total discharge of the hydro units over the planning period must be equal to the pre-specified water volume of the reservoir as given in Eq. (6).

(iv) The water volume of pumped storage units

The pumped storage reservoir's initial water volume must equal the reservoir's final water volume, as given in Eq. (12)

(v) Output power generation bounds

The output power generation limit of each thermal, hydro, pumped storage, and solar generator during the feasible operation of the described power system is provided as follows:

$$P_i^L \leq P_{ti} \leq P_i^U \qquad \left(i \in \left[1, N_t + N_h + N_p\right]; t \in [1,T]\right) \tag{22}$$

$$0 \leq P_{tk}^S \leq P_k^U \qquad (t \in [1,T]; k \in [1,N_s]) \tag{23}$$

(vi) Spinning Reserves

According to Wood (1982), the spinning reserve is the unused capacity that connected devices can use to influence active power. 10% of the power needed for spinning reserves is taken into account in this work. So, '*x*' is set to 0.1.

$$\left(\sum_{j=1}^{N_g} min\left(\left(P_j^U - P_{tj}\right), UR_j\right)\right) \geq xP_{Dt} \tag{24}$$

3. COMMITMENT OF SOLAR UNITS

Solar power share should not exceed certain demand limits to maintain the uninterrupted supply. Solar units are quick-to-start units and have uncertain sun radiation, respectively. If the available number of solar units is more than the required number, and their share exceeds the certain limits of demand, then the commitment of units is required. The commitment to solar units is stated in t^{th} time below.

The minimum operating cost of solar power at the time, t [58]:

$$\text{Minimize}(\mathrm{F}_t^S) = \sum_{n=1}^{N_s}\left((C_n^S \mathrm{P}_{tn}^S \mathrm{U}_{tn}^S)\right) {}^{\$}/_{h} \tag{25}$$

Subject to:

(i) solar power share limits from the committed units are given below:

$$\sum_{n=1}^{N_s} \mathrm{U}_{tn}^S P_{tn}^S \leq \lambda P_t^D \qquad (t \in [1,T]) \tag{26}$$

(ii) The limits of committed wind and solar generators are:

$$P_n^{S^L} \le \mathrm{U}_{tn}^S P_{tn}^S \le P_n^{S^U} \quad \left(n \in [1, N_s]; (t \in [1, T])\right) \tag{27}$$

where U_{tn}^S are binary variable that gives the status of committed solar power units at time, t. '1' status gives the committed (ON) unit, and 0 is for de-committed (OFF) units.

3.1. Computational Steps for Commitment of Solar Units

Because solar power output is intermittent and unpredictable, it is necessary to commit the solar generating units via an optimistic one-point crossover [59]. The power from these units is expected to be accessible at that moment. The steps are outlined below:

Initialization: Solar units, by using the following mathematical relation, are randomly committed/de-committed:

$$U_{ktn}^S = \begin{cases} 1 & ; r_d \ge 0.5 \\ 0 & ; r_d < 0.5 \end{cases} \quad (n \in [1, N_S]; t \in [1, T]; k \in [1, n_s]) \tag{28}$$

where rand () is a uniform random number and $\in [0,1]$

Fitness evaluation: The operating cost of solar generators is calculated with the sustainable region and is referred to as the fitness value for the system, with limits incorporated using a penalty factor.

$$A_{kt} = F_{kt}^S + R_k\left(\sum_{n=1}^{N_s} U_{tn}^S P_{tn}^S - \lambda P_{Dt}\right) (k \in [1, n_s]; t \in [1, T]) \tag{29}$$

where R_k is an exterior penalty factor and set to a large value.

Crossover: The commitment table has been updated using a very optimistic minimization procedure. Arrange all members following their increasing fitness value. The first half is considered the better population, while the second half is considered the worst population. Members of the better half of the population are exchanged for members of the worst half of the population. The exchange only $N_s - j$ characteristics of the member.

$$U_{ktn}^S \leftrightarrow U_{ltn}^S \quad \left(n \in [j_r, N_s]; t \in [1, T];\ k \in \left[1, \tfrac{n_s}{2}\right], l = k + \tfrac{n_s}{2}\right) \tag{30}$$

De-commitment of Units: when $\sum_{n=1}^{N_s} P_{ktn}^S U_{ktn}^S > \lambda P_{Dt}$ it is needed to de-commit the randomly selected committed unit among solar units until $\sum_{i=1}^{N_s} P_{kti}^S U_{kti}^S \le \lambda P_{Dt}$. The de-commitment procedure is defined below:

$$U_{ktm}^S = \begin{cases} 0 & ; U_{ktm}^S = 1 \text{ and} \left(\sum_{n=1}^{N_s} P_{ktn}^S U_{ktn}^S > \lambda P_{Dt}\right) \\ \text{no change} & ;\ \text{otherwise} \end{cases} \quad (k \in [1, n_s]) \tag{31}$$

where m is a random integer $\in [1, N_s]$

Stopping Criterion: The proposed optimization technique ends when the specified number of iterations is completed, and the upgraded best operating cost is recorded.

The constraints imposed on the generation scheduling problem are handled using the direct search heuristic method. The constraints handling procedure is discussed in detail.

4. PROCEDURE TO ATTAIN A FEASIBLE SOLUTION

The multiobjective hybrid energy generation scheduling (HEGS) problem is subjected to a certain set of physical and operational constraints. These constraints include output power violation and meeting the load demand with the transmission losses. The following equations are used to satisfy the above-mentioned constraints.

4.1. Managing inequality constraints

During the search, a replacement method is used to restraint the power generation within the limit of the i^{th} generator:

$$P_{ki} = \begin{cases} P_{ki}; (P_i^L \le P_{ki} \le P_i^U) \\ P_i^L \quad ; (P_{ki} < P_i^L) \\ P_i^U \quad ; (P_{ki} > P_i^U) \end{cases} \qquad (i \in [1, N_g]; k \in [1, T]) \tag{32}$$

4.2. To utilize the available water volume

An iterative repair technique is used to manage the equality restrictions based on the proportional sharing of the water utilized by hydro units during each sub-interval. The following formula is used to compute the difference between the total water volume in the reservoir and the total water discharge rate.

$$E_j^v = V_j - \sum_{t=1}^{T} t_t q_{tj} \qquad (j \in [1, N_h]) \tag{33}$$

When the value of $|E_j^v| \le \epsilon$ the reservoir's overall storage is utilized to its greatest potential; otherwise, power generation is updated to increase or decrease its value using the following equation.

$$P_{t,j+N_t} = \begin{cases} P_{t,j+N_t} + \min\left((P_j^U - P_{t,j+N_t}) r_j, \ \left(\frac{|E_j^v|}{\sum_{t=1}^{T} q_{kj}} \right) P_{t,j+N_t} \right) ; (E_j^v > 0) \\ P_{t,j+N_t} - \min\left((P_{t,j+N_t} - P_j^L) r_j, \ \left(\frac{|E_j^v|}{\sum_{t=1}^{T} q_{tj}} \right) P_{t,j+N_t} \right) ; (E_j^v < 0) \end{cases} \tag{34}$$

$(j \in [1, N_h]; t \in [1, T])$

4.3. Technique to utilize the available water volume of pumped storage hydro unit

The difference between the beginning volume and end volume of the pumped storage units is measured using the following equation, which is represented by E_l^{PS}

$$E_l^{PS} = V_l^F - V_l^I - (\sum_{t=1}^{T} t_t q_{tl}^+ - \sum_{t=1}^{T} t_l |q_{kl}^-|) \qquad (l \in [1, N_p]; t \in [1, T]) \tag{35}$$

Two pumped storage discharge variables R_{Gl} and R_{Pl} are selected for the pumping and generation mode of pumped storage units, respectively.

$$R_{Gl} = \frac{\sum_{t=1}^{T} t_t q_{tl}^+}{\sum_{t=1}^{T} t_t |q_{tl}^+| + \sum_{t=1}^{T} t_t |q_{tl}^-|} \qquad (l \in [1, N_p]) \tag{36}$$

$$R_{Pl} = \frac{\sum_{k=1}^{T} t_k \left| q_{kj}^{-} \right|}{\sum_{t=1}^{T} t_t |q_{tl}^{+}| + \sum_{t=1}^{T} t_t |q_{tl}^{-}|} \qquad \left(l \in [1, N_p] \right) \tag{37}$$

In case, $\left| E_l^{PS} \right| \leq \epsilon$ the reservoir's overall storage is then used to its maximum capacity. The power output of pumped storage units is modified within its limits using the following equations for pumping as well as generation mode.

$$P_{tl} = \begin{cases} P_{tl} + \min\left((P_l^U - P_{tl}) r_j, R_{Pl} \left(\frac{\left| E_l^{PS} \right|}{\sum_{t=1}^{T} t q_{tj}^{+}} \right) |P_{tl}| \right); (\sigma_G \text{ and } E_l^{PS} > 0) \\ P_{tl} - \min\left(\left(P_{tl} - P_j^L \right) r_j, R_{Gl} \left(\frac{\left| E_l^{PS} \right|}{\sum_{t=1}^{T} t_t |q_{tl}^{-}|} \right) |P_{tl}| \right); (\sigma_G \text{ and } E_l^{PS} < 0) \end{cases}$$

$$\left(l \in \left[N_t + N_h + 1, N_t + N_h + N_p \right]; t \in [1, T] \right) \tag{38}$$

$$P_{tl} = \begin{cases} P_{tl} - \min\left((P_{tl} - P_l^L) r_j, R_{Gl} \left(\frac{\left| E_l^{PS} \right|}{\sum_{t=1}^{T} t_t |q_{tl}^{-}|} \right) |P_{tl}| \right); (\sigma_P \text{ and } E_l^{PS} > 0) \\ P_{tl} + \min\left((P_m^U - P_{tl}) r_j, R_{Pl} \left(\frac{\left| E_l^{PS} \right|}{\sum_{t=1}^{T} t_t q_{tl}^{+}} \right) |P_{tl}| \right); (\sigma_P \text{ and } E_l^{PS} < 0) \end{cases} \tag{39}$$

$$\left(l \in \left[N_t + N_h + 1, N_t + N_h + N_p \right]; t \in [1, T] \right)$$

4.4. To meet the load demand

The power mismatch for the generation schedules during each sub-interval is calculated using the following equation and is indicated by E_t^{PD}.

$$E_t^{PD} = P_t^D + P_t^{Loss} \; - \sum_{i=1}^{N_g} P_{ti} \qquad (t \in [1, T]) \tag{40}$$

When the value of $|E_t^{PD}| \leq \epsilon$ the generated power is within the feasible range, and the solution does not need to be repaired. Within generation limits, the solution is repaired using the following equation based on proportional sharing of unmet demand to each generator.

$$P_{ti} = \begin{cases} P_{ti} + \min\left((P_i^U - P_{ti}) r_i, \; \left(\frac{|E_t^{PD}|}{\sum_{i=1}^{ng} P_{ti}} \right) P_{ti} \right) \; ; (E_t^{PD} > 0) \\ P_{ti} - \min\left((P_{ti} - P_i^L) r_i, \; \left(\frac{|E_t^{PD}|}{\sum_{i=1}^{ng} P_{ti}} \right) P_{ti} \right) ; (E_t^{PD} < 0) \end{cases} \tag{41}$$

$$(i \in [1, N_t + N_h]; t \in [1, T])$$

The feasible solution should satisfy the following equation so that equations (33), (35), and (40) are satisfied.

$$E = \left(\sum_{j=1}^{N_h} \left(E_j^v \right)^2 + \sum_{l=1}^{N_p} (E_l^{PS})^2 + \sum_{t=1}^{T} (E_t^{PD})^2 \right)^{1/2} \; \leq \epsilon \tag{42}$$

where ϵ is a small positive value closer to zero.

5. EMENDED SNAKE OPTIMIZER (ESO)

The proposed emended snake optimizer (ESO) is used to explore the constrained multiobjective hybrid energy generation scheduling (HEGS) problem. For improved performance, the basic snake optimization algorithm is combined with the simplex search technique. The primary idea of ESO is to conduct real-world research into snake mating behaviour. Snakes are scaled, cold-blooded reptiles with no legs. Snakes have extended bodies and tails and lack limbs. Three thousand six hundred snake species are divided into 520 genera and 20 snake families. Almost all snakes have skulls with several joints, allowing them to swallow prey larger than their heads. Snakes have a distinct mating behaviour. They mate in the early and late summer seasons. When a male snake travels far during mating season in search of a female, the mating process begins. Males can travel in large groups and engage in physical altercations or confrontations with one another over a female snake on occasion. Mating is mostly determined by the availability of food and the temperature. A sufficient amount of food and a cold temperature leads to mating; otherwise, snakes look for food or eat what is already there. Exploration and exploitation are the two stages of the search process. When no appropriate amount of food is available during the exploration phase, snakes migrate solely in search of food. The exploitation step encompasses several phases to obtain a global solution. Snakes take food when it is accessible, but the temperature is high. Snakes mate when food is available, and the weather is cold.

There are two modes of mating: fight mode and mating mode. Male snakes will battle to get the best female in fight mode. When snakes fight, they bite each other. These reptiles compete for the fertilization of a single female snake, believed to be a receptive female. Depending on the female's acceptability, the fight's winner will mate. After mating, the female lays eggs and departs as soon as the eggs hatch into baby snakes. The steps in SOA are described below [49].

5.1. Initialization

The snake population is generated randomly, the initial feasible solution in the search space. Within the limits of hydrothermal power output generation, an initial population of snakes (P_{kti}) is formed at random as follows:

$$P_{kti} = P_i^L + (P_i^U - P_i^L) r_{kti} \qquad \left(i \in [1, \mathrm{N}_g]; t \in [1, T];\ k \in [1, n_\mathrm{s}]\right) \tag{43}$$

n_s is the population of snakes and n_g(n+m) is the total number of hydro and thermal generators. To begin the optimization algorithm, a matrix of size $\left(n_\mathrm{s} \times \mathrm{T} \times n_g\right)$ is generated randomly as:

$$P_k(g) = \begin{bmatrix} P_{k11}(g) & P_{k12}(g) & \cdots & \cdots & P_{k1n_g}(g) \\ P_{k21}(g) & P_{k22}(g) & \cdots & \cdots & P_{k2n_g}(g) \\ \vdots & \vdots & \vdots & \vdots & \vdots \\ P_{kT1}(g) & P_{kT2}(g) & \cdots & \cdots & P_{kTn_g}(g) \end{bmatrix}_{T \times N_g} \quad (k \in [1, n_\mathrm{s}])$$

The objective function $F_k(g)$of each snake can be calculated as:

$$F_k(g) = F\left(P_k(g)\right) \quad (k \in [1, n_\mathrm{s}]) \tag{44}$$

5.2. Categorization of Male and Female Snakes

Males and females compose the total population. Each group accounts for half of the entire population. The population of snakes, n_s is equally divided into males, n_l and females, n_o. The male, $X_k(g)$ and female, $Y_k(g)$ population and corresponding objective function of male $F_k^X(g)$ and female, $F_k^Y(g)$ are represented as vectors of snakes as $P_k(g) = [X_k(g) : Y_k(g)]^T$ and $F_k(g) = [F_k^X(g) : F_k^Y(g)]^T$. The iteration counter is represented by g.

5.3. Temperature and Food Quantity

The temperature and availability of food influences snake mating. The temperature T_{temp} and food quantity Q are defined below:

$$T_{temp} = exp\left(\frac{-g}{G^{max}}\right) \tag{45}$$

$$Q = C_1 exp\left(\frac{g - G^{max}}{G^{max}}\right) \tag{46}$$

where g and G^{max} refers to the current iteration and the maximum number of iterations. $C_1$is constant and set equals to 0.5.

5.4. Exploration Phase

Food is scarce during the exploratory phase, so snakes forage. If Q is less than the chosen threshold value for available food, snakes will hunt for it by selecting any random spot and updating their positions in relation to it. If $Q < 0.25$ then the exploration phase is modelled as follows.

$$P_{kti}(g+1) = \begin{cases} Y_{uti}(g) \pm C_2\left(exp\left(-\frac{F_u^Y(g) - F^{best}(g)}{F_k^X(g) - F^{best}(g) + \epsilon}\right)\right)\left((P_i^L - P_i^U)r_i + P_i^L\right);\ r < 0.6 \\ X_{uti}(g) \pm C_2\left(exp\left(-\frac{F_v^X(g) - F^{best}(g)}{F_k^Y(g) - F^{best}(g) + \epsilon}\right)\right)\left((P_i^U - P_i^L)r_i + P_i^L\right);\ r \geq 0.6 \end{cases}$$

$$\left(i \in [1, N_g]; t \in [1, T]; k \in [1, n_s]\right) \tag{47}$$

where $P_{kti}(g+1)$ is the k[th] snake position, $X_{uti}(g)\ and\ Y_{uti}(g)$ represents the random positions of male and female snakes, respectively during the $(g+1)^{th}$ movement and $v \in [1, n_l]$ and $u \in [1, n_o]$ are random integers. C_2 is a constant and set equal to 0.05. r_i is a random number between 0 and 1. $F_v^X(g)$ and $F_u^Y(g)$ refers to the fitness of random male and female snakes. The exponent term considers the decreasing ratio of the fitness distances of solutions from the best solution so that the factor plays an effective role in updating the variables. ϵ is a small value to ensure that the denominator does not lead to zero.

5.5. Exploitation Phase

The exploitation phase occurs when the food amount exceeds the threshold value (Q>threshold), indicating that food exists. When the temperature is high (higher than the

threshold (0.6), or when the temperature is high, there is no mating, and snakes will only migrate towards food, as indicated by the following equation:

$$P_{kti}(g+1) = P_{uti}(g) \pm C_3 T_{temp}\left(P_{ti}^{best} - P_{kti}(g)\right) r_i$$

$$\left(i \in [1, N_g]; t \in [1, T]; k \in [1, n_s]\right) \quad (48)$$

where P_{ti}^{best} refers to the position of the best snake and C_3 is a constant equal 3.u is a random integer $\in [1, n_s]$.

When the temperature is low or chilly, it implies the temperature is less than the threshold of 0.6, and snakes will be in fight or mating mode for male and female snakes, respectively. In fight mode, each male snake competes for the best female snake, while each female snake chooses the best male snake. The fighting mode for male and female snakes is indicated mathematically below:

$$X_{kti}(g+1) = X_{kti}(g) \pm \left(exp\left(-\frac{(F_Y^{best} - F^{best}(g))}{(F_k^X(g) - F^{best}(g) + \epsilon)}\right)\right)\left(QY_{ti}^{best} - X_{kti}(g)\right) r_i$$

$$\left(i \in [1, N_g]; t \in [1, T]; k \in [1, n_l]\right) \quad (49)$$

$$Y_{kti}(g+1) = Y_{kti}(g) \pm \left(exp\left(-\frac{(F_X^{best} - F^{best}(g))}{(F_k^Y(g) - F^{best}(g) + \epsilon)}\right)\right)\left(QX_{ti}^{best} - Y_{kti}(g)\right) r_i$$

$$\left(i \in [1, N_g]; t \in [1, T]; k \in [1, n_o]\right) \quad (50)$$

where F_Y^{best} and F_X^{best} represents the fitness of the best female and best male, respectively. F_k^X and F_k^Y represents the fitness of k^{th} female and male agents, respectively.

Mating happens between each pair based on the quantity of food available during cold weather scenarios. The mating mode is given mathematically below.

$$X_{kti}(g+1) = X_{kti}(g+1) \pm \left(exp\left(-\frac{(F_k^Y(g) - F^{best}(g))}{(F_k^X(g) - F^{best}(g) + \epsilon)}\right)\right)\left(QX_{kti}(g) - Y_{kti}(g+1)\right) r_I$$

$$\left(i \in [1, N_g]; t \in [1, T]; k \in [1, n_l]\right) \quad (51)$$

$$Y_{kti}(g+1) = Y_{kti}(g+1) \pm \left(exp\left(-\frac{(F_k^X(g) - F^{best}(g))}{(F_k^Y(g) - F^{best}(g) + \epsilon)}\right)\right)\left(QY_{kti}(g) - X_{kti}(g+1)\right) r_I$$

$$\left(i \in [1, N_g]; t \in [1, T]; k \in [1, n_o]\right) \quad (52)$$

Where $F_k^X(g)$ and $F_k^Y(g)$ are the fitness of k^{th} male and k^{th} female agents, respectively. Choose the worst male and female and replace them if the egg incubates.

$$P_{kti}^{worst} = P_i^L + (P_i^U - P_i^L)r_i \quad \left(i \in [1, N_g]; t \in [1, T]; k \in [1, n_s]\right) \tag{53}$$

Where P_{kti}^{worst} represents the position of worst snake and is divided into two equal parts of worst male and female position and is represented by P_l^{worst} and P_o^{worst}, respectively.

5.6. Simplex Search Method

Nelder and Mead's simplex approach is an extension of the method proposed by Spendley et al. [60]. This approach is a local search strategy that exploits the geometric qualities of the n-dimensional space to construct a simplex in an n-dimensional space (N_g+1) The four basic operations are reflection, expansion, contraction, and shrinkage, and they are used to rescale the simplex based on the function's local behaviour. The simplex can successfully improve itself and thrive closer to the optimal solution through these steps. To begin, choose the worst snake agent $\left(P_{l_1 t}\right)$, the best agent $\left(P_{l_2 t}\right)$ and the next worst agent $\left(P_{l_3 t}\right)$ from the initial set of snake agents. Calculate the centroid (P_{ti}^C) of all snake agents using the formula:

$$P_{ti}^C = \frac{1}{n_s}\sum_{k=1, k\neq l_1}^{n_s+1} P_{kti} \qquad \left(i \in [1, N_g]; t \in [1, T]\right) \tag{54}$$

The new reflected agent, P_{ti}^R, is computed as follow:

$$P_{ti}^R = \gamma P_{ti}^C - P_{l_1 ti} \qquad \left(i \in [1, N_g]; t \in [1, T]\right) \tag{55}$$

The new position of snake is computed as given below:

$$P_{ti}^N = \begin{cases} (1+\alpha)P_{ti}^C - \alpha P_{l_1 ti} & ; F(P^R) < F\left(P_{l_2}\right) \quad \text{(Expansion)} \\ (1-\beta)P_{ti}^C - \gamma P_{l_1 ti} & ; F(P^R) \geq F\left(P_{l_1}\right) \quad \text{(insideContraction)} \\ (1+\beta)P_{ti}^C + \gamma P_{l_1 ti} & ; F\left(P_{l_3}\right) < F(P^R) < F\left(P_{l_1}\right) \quad \text{(outside contraction)} \\ P_{ti}^R & ; otherwise \end{cases} \tag{56}$$

$$\left(i \in [1, N_g]; t \in [1, T]\right)$$

A better one is selected, and a new simplex is formed. The process can be terminated if no improvement is observed in the objective function. i.e. $\left|F(P_{ti}^N) - F^G\left(P_{ti}^{best}\right)\right| \leq \epsilon$. ϵ is the termination parameter.

5.7. Opposition based learning

Certain randomly generated starting solutions are necessary in order to improve the optimal point in heuristic optimization methods. The time it takes to calculate the optimal solution is affected by the distance between the initial and optimal solutions. Starting with a better solution and comparing it to its opposite solution can help to reduce computing time. Iteration begins with selecting the initial solution, which is either the opposite of the original solution or the better alternative from the initial guess. In probability theory, there are half chances, and a hypothesis is closer to the solution than its inverse hypothesis. Opposition-based learning considers quasi-opposite, quasi-reflection, extended opposite, and reflected opposite numbers to find improved solutions to the hybrid energy generation scheduling problem.

Opposing numbers are considered in opposition-based learning. Each variable is reflected across the center of its search area when computing an opposite number. The snakes are forming on the opposite number using the following equation:

$$P^{o}_{ktj}(g) = P^{UL}_{tj}(g) + P^{LL}_{tj}(g) - P_{ktj}(g) \qquad \left(j \in [1, N_g]; t \in [1, T]; k \in [1, n_s]\right) \tag{57}$$

where,

$$P^{LL}_{tj}(g) = \begin{cases} min(P_{ktj}(g) \;\; ; k \in [1, n_s]) & ; rand > \dfrac{g}{G^{max}} \\ P^{L}_{j} & ; otherwise \end{cases}$$

$$P^{UL}_{tj}(g) = \begin{cases} max(P_{ktj}(g) \;\; ; k \in [1, n_s]) & ; rand < \dfrac{g}{G^{max}} \\ P^{U}_{j} & ; otherwise \end{cases}$$

Each variable is randomly reflected between its search space and the variable itself in quasi-reflected opposition. As expressed mathematically,

$$P^{01}_{ktj} = P_{ktj} + rand(d_{tj} - P_{ktj}) \quad \left(j \in [1, N_g]; t \in [1, T]; k \in [1, n_s]\right) \tag{58}$$

where, $d_{tj} = \frac{P^{UL}_{tj} + P^{LL}_{tj}}{2} \; \left(j \in [1, N_g]; t \in [1, T]\right)$

Quasi-opposition moves each variable to a random point from the middle of its search space and its opposite number and, mathematically, stated as

$$P^{02}_{ktj} = d_{tj} + rand\left(P^{o}_{ktj} - d_{tj}\right) \qquad \left(j \in [1, N_g]; t \in [1, T]; k \in [1, n_s]\right) \tag{59}$$

Extended opposition shifts each variable to a random point between its opposite number and the nearest bound of its search space to its opposite number.

$$P^{03}_{ktj} = \begin{cases} P^{o}_{ktj} + rand(P^{UL}_{tj} - P^{o}_{ktj}); & P^{o}_{ktj} < d_{tj} \\ P^{LL}_{tj} + rand(P^{o}_{ktj} - P^{LL}_{tj}); & else \end{cases} \quad \left(j \in [1, N_g]; t \in [1, T]; k \in [1, n_s]\right) \tag{60}$$

Reflected Extended Opposition reflects the extended opposite point to compute the reflected extended opposite point and, mathematically, stated as

$$P^{04}_{ktj} = \begin{cases} P_{ktj} + rand\left(P^{UL}_{tj} - P_{ktj}\right); & P_{ktj} > d_{tj} \\ P^{LL}_{tj} + rand(P_{ktj} - P^{LL}_{tj}); & else \end{cases} \quad \left(j \in [1, N_g]; t \in [1, T]; k \in [1, n_s]\right) \tag{61}$$

Out of available $2n_s$ snakes, best n_s snakes are retained for further improvement after applying each opposition move [61].

Comprehensive Opposition The comprehensive opposition shifts the variable to one of its opposite points P^{o4}_{ki}, P^{o3}_{ki}, P^{o1}_{ki} or P^{o2}_{ki} whose probability of being selected are $E_1, E_2, E_3 and E_4$, respectively [62]. In other words, it can be defined as given below:

$$P^{co}_{ki} = \begin{cases} P^{O4}_{ki} & ; r \le E_1 \\ P^{01}_{ki} & ; E_1 < r \le E_1 + E_2 \\ P^{o2}_{ki} & ; E_1 + E_2 < r \le E_1 + E_2 + E_3 \\ P^{03}_{ki} & ; E_1 + E_2 + E_3 < r \le 1 \end{cases} \tag{62}$$

where rand is a random number uniformly distributed in [0,1] and the optimum values of the parameters of E_1, E_2, E_3 and E_4 are probabilities to be adjusted. After applying each opposition move, the best agents are retained from among those available for further improvement.

Calculation of time complexity: The time complexity has also been analyzed in the current work. Number function evaluations can be computed as $NFE = n_S + G^{max}(n_S + 2G_s^{max})$. The complexity order is 2. The complexity order is 2. The addition of a simplex search strategy and opposition-based learning adds the function evaluations, which results in more time consumption to perform the algorithm but improves the algorithm's performance.

The stepwise procedure of the emended snake optimizer (ESO) is outlined in algorithm I.

Algorithm-I Stepwise procedure of hybrid snake optimizer (ESO)

Inputs

n, m, n_S, n_l, n_o, Total number of iterations, $G^{\max}$
P^U, P^L, $P_t^D(t \in [1,T])$, a_i, b_i, c_i , d_i and $e_i(i \in [1,N_t])$, x_j,y_j and $z_j(j \in [1,N_h])$, α_j,β_j and $\gamma_j(j \in [1,N_h])$

Initialize snakes population using Eq. (43)

Find a feasible solution while satisfying Eq. (33), Eq. (35), Eq. (40), and Eq. (42)

Compute fitness of snake members using Eq. (44)

Divide the population n_S into two equal groups n_l and n_o

Divide the fitness of male and female agents as step 5.

Compute the best fitness value of the best male,$F_X^{best} min\{F_k^X(g); k \in [1,n_l]\}$and female snake agent, $F_Y^{best} min\{F_k^Y(g); k \in [1,n_o]\}$.

Compute the global fitness value, $F^{best} = min\{F_X^{best}, F_X^{best}\}$ and $P_{ti}^{best}; i \in [1,N_g]; t \in$

Set counter $g = 1$

WHILE ($g \leq G^{\max}$) **DO**

  Define T_{Temp}, temperature using Eq. (45)

  Define food quantity Q using Eq. (46)

  IF$(\mathbf{Q} < 0.25)$**THEN**

  Perform exploration using Eqs.(47)

  ELSE IF$(\mathrm{Q} > 0.25)$**THEN**

  Perform exploitation using Eq. (48)

  ELSE

    IF$(\mathrm{rand} > threshold\ (0.6))$**THEN**

    Snakes in fight mode using Eqs. (49) and (50)

    ELSE

    Snakes in mating mode using Eqs. (51) and (52)

Update the worst male and female using Eq. (53)
END IF
END IF
Find a feasible solution while satisfying Eq. (33), Eq. (35), Eq. (40), and Eq. (42)
Compute fitness of snake members, $F_k^X(g)$ and $F_k^Y(g)$using Eq. (44)
Find $F_X^{best} = min\{F_k^X(g); k \in [1, n_l]\}$ and Find $F_Y^{best} = min\{F_k^Y(g); k \in [1, n_o]\}$
Find $F^{nbest} = min\{F_X^{best}, F_X^{best}\}$ and P^{nbest}
IF ($F^{nbest} < F^{best}$)**THEN**
Update $F^{best} \leftarrow F^{nbest}$ and $P_{ti}^{best} \leftarrow P_{ti}^{nbest}; i \in [1, N_g]; t \in [1, T]$
ENDIF
Set counter $g_1 = 1$
WHILE ($g_1 \leq G_s^{max}$**) DO (**Simplex Search Method)
Determine worst snake (P_{l_1}), the best snake (P_{l_2}) and next to the worst agent (P_{l_3})
Computer agent at centroid, P_{ti}^C using Eq.(54)
Compute new reflected agent, P_{ti}^R using Eq. (55)
Find a feasible solution while satisfying Eq. (33), Eq. (35), Eq. (40), and Eq. (42)
Compute fitness of snake member, $F^R(P^R)$ using Eq. (44)
Perform expansion, inside, and outside contraction to locate the new position P_{ti}^N, of the snake agent using Eq. (56).
Find a feasible solution while satisfying Eq. (33), Eq. (35), Eq. (40), and Eq. (42)
Compute fitness of snake member, $F^N(P^N)$ Eq. (44)
Replace worst function value with new function $F^{l_1}(P_{l_1}) \leftarrow F^N(P^N)$ and $X_{ti}^H \leftarrow P_{l_1 ti}^N i \in [1, N_g]; t \in [1, T]$
IF($F^N < F^{best}$)**THEN**
Update $F^{best} \leftarrow F^N$ and $P_{ti}^{best} \leftarrow P_{ti}^N; i \in [1, N_g]; t \in [1, T]$
ENDIF
IF (The termination criterion is met) **THEN EXIT**
Increment counter$g_1 = g_1 + 1$
END WHILE
Apply opposition based learning using Eqs. (57-62)
Increment counter$g = g + 1$
END WHILE
STOP

6. RESULTS AND DISCUSSIONS

The results of the standard benchmark optimization problems (unconstrained unimodal, multimodal) and scalar and bi-objective hydrothermal generation scheduling problems

with pumped storage and solar generating units using an emended snake optimizer are discussed in this section.

6.1. Standard benchmark optimization problems

The proposed emended snake optimizer (ESO) algorithm's viability is examined on 13 standard benchmark optimization problems. The parameters of ESO are selected by performing simulation and are given in Table 1. Some of the solar power generation parameters for coordinated generation are given in Table 2.

Table 1: Parameters of ESO

Parameter	Value	Parameter	Value
Dimension, D	10	Control parameter, C_1	0.5
Population, n_s	30	Control parameter, C_2	0.05
Maximum iterations, G^{max}	100	Control parameter, C_3	3
Maximum iteration, for simplex, G_s^{max}	250	Independent trial number of N-run	30

***Parameter tuning**:* In the simplex search strategy, the considered value for the expansion factor (γ) is 2, and for contraction (β), the factor is 0.5 for undertaken HEGS problems. The control parameters of ESO are C_1, C_2, and C_3. The next and most important parameter is the population of snakes (n_s). Variations in the snake population impact the algorithm's performance. Therefore, several experiments have been done on these parameters, and their best value for test systems is given in Table 1. Table 2 gives the solar power system parameters used for coordinated generation. The definitions of standard benchmark functions are given in Table 3.

Table 2: Solar power generation system parameters

PARAMETER	**VALUE**	**PARAMETER**	**VALUE**
β (tilt angle)	30°	η_w(PV array wiring efficiency)	98%
d (day number)	135 (15th May)	T_c^P(cell temperature)	50°C
δ (declination angle)	23.371 radian	T_r^P(temperature of the cell at a reference temperature)	25°C
Φ (Latitude of location)	28.7041 (Delhi)	T_n^{not}normal operating cell temperature)	45°C
σ(constant)	0.144	Z(temperature coefficient of the solar cell)	-0.004 °C^{-1}
C(constant)	0.071	S(insolation)	80(mW/cm^2)
η_e(efficiency of PV array)	11%	ρ(ground reflectivity)	0.20
η_d(factor of degradation)	90%	A(surface area of the PV array)	90900 m^2
η_r(efficiency of a solar cell at a reference solar radiation)	10.5%	μ(constant)	1215
η_c(efficiency of the power conditioning devices)	99%		

Table 3: Definitions of standard benchmark optimization problems

No.	Name	Mathematical expression of the objective function	Range	f_{min}
$f_1(x)$	Sphere	$f_1(x) = \sum_{i=1}^{n} x_i^2$	[-100,100]	0
$f_2(x)$	Schwefel's 2.22	$f_2(x) = \sum_{i=1}^{n} \lvert x_i \rvert + \prod_{i=1}^{n} \lvert x_i \rvert$	[-10,10]	0
$f_3(x)$	Schwefel's 1.2	$f_3(x) = \sum_{i=1}^{n} \left(\sum_{j-1}^{i} x_j \right)^2$	[-100,100]	0
$f_4(x)$	Schwefel's 2.21	$f_4(x) = max(\lvert x_i \rvert, 1 \le i \le n)$	[-100,100]	0
$f_5(x)$	Rosenbrock	$f_5(x) = \sum_{i=1}^{n-1} [100(x_{i+1} - x_i^2)^2 + (x_i - 1)^2]$	[-30,30]	0
$f_6(x)$	Step	$f_6(x) = \sum_{i=1}^{n} (\lvert x_i + 0.5 \rvert)^2$	[-100,100]	0
$f_7(x)$	Quartic	$f_7(x) = \sum_{i=1}^{n} i x_i^4 + random[0,1)$	[-1.28,1.28]	0
$f_8(x)$	Rastrigin	$f_8(x) = \sum_{i=1}^{n} -x_i sin\left(\sqrt{\lvert x_i \rvert}\right)$	[-500,500]	-418.98D
$f_9(x)$	Schwefel's 2.26	$f_9(x) = \sum_{i=1}^{n} [x_i^2 - 10\cos(2\pi x_i) + 10]$	[-5.12,5.12]	0
$f_{10}(x)$	Ackley	$f_{10}(x) = -20exp\left(-0.2\sqrt{\frac{1}{N}\sum_{i=1}^{N} x_i^2}\right) - exp\left(-\frac{1}{N}\sum_{i=1}^{N} cos(2\pi x_i)\right) + 20 + e$	$[-32,32]$	0
$f_{11}(x)$	Griewank	$f_{11}(x) = \sum_{i=1}^{n} \frac{1}{4000}\sum_{i=1}^{n} x_i^2 - \prod_{i=1}^{n} cos\left(\frac{x_i}{\sqrt{i}}\right) + 1$	[-600,600]	0
$f_{12}(x)$	Penalized	$f_{12}(x) = \frac{\pi}{N}\left\{10\sin(\pi y_i)\right\} + \frac{\pi}{N}\left\{\sum_{i=1}^{N-1}(y_i - 1)^2[1 + 10sin^2(\pi y_{i+1})]\right\} + \sum_{i=1}^{N} u(x_i, a, k, m)$ $y_i = 1 + \frac{x_i+1}{4}$ $u(x_i, a, k, m) = \begin{cases} k(x_i - a)^m & x > a \\ 0 - a & < x_i < a \\ k(-x_i - a)^m & x_i < -a \end{cases}$	$[-50,50]$	0
$f_{13}(x)$	Penalized 2	$f_{13}(x) = 0.1\{sin^2(3\pi x_1) + \sum_{i=1}^{N}(x_i - 1)^2[1 + sin^2(3\pi x_i + 1)] + \frac{1}{2}(x_N - 1)^2[1 + sin^2(2\pi x_N)]2\} + \sum_{i=1}^{N} u(x_i, 5,100,4)$	$[-50,50]$	0

The average, median, minimum, maximum, and standard deviation values of standard benchmark functions for SOA and ESO are tabulated in Table 4. The comparison of results for ESO with other techniques viz. particle swarm optimization (PSO), genetic algorithm

(GA), differential evolution (DE), Harris hawk optimizer (HHO) and biogeography-based optimization (BBO) present in literature [63] is given in Table 5. This comparison shows that the proposed ESO gives better results than other techniques for all standard benchmark functions. Hence it is concluded that ESO performs better than SOA and other techniques. Friedman's test is performed to validate the results, and ESO got the first rank among all competing algorithms.

Table 4: Performance analysis of SOA and ESO on standard benchmark optimization problems

Test Function	Algorithm	Objective Function Value				Stdev
		Average	Median	Minimum	Maximum	
$f_1(x)$	SOA	8.259E-297	8.14E-297	5.94E-297	9.9E-297	0
	ESO	**7.7802E-297**	**8.06E-297**	**5.77E-297**	**9.2526E-297**	**0**
$f_2(x)$	SOA	4.683E-149	4.635E-149	3.77E-149	6.19E-149	4.8E-150
	ESO	**4.5523E-149**	**4.5007E-149**	**3.1486E-149**	**5.6457E-149**	**4.8E-150**
$f_3(x)$	SOA	1.1313E-297	1.135E-297	8.91E-298	1.38E-297	0
	ESO	**1.1004E-297**	**1.0772E-297**	**8.3147E-298**	**1.4532E-297**	**0**
$f_4(x)$	SOA	2.962E-150	2.98E-150	2.58E-150	3.27E-150	1.6E-151
	ESO	**2.8932E-150**	**2.9352E-150**	**2.5757E-150**	**3.2044E-150**	**1.6E-151**
$f_5(x)$	SOA	28.99468	28.99889	28.94956	29	0.010237
	ESO	**28.7396**	**28.75511**	**28.50983**	**28.82333**	**0.040035**
$f_6(x)$	SOA	0	0	0	0	0
	ESO	**0**	**0**	**0**	**0**	**0**
$f_7(x)$	SOA	1.73E-04	1.82E-04	1.29E-04	1.82E-04	1.98E-05
	ESO	**1.30E-04**	**1.29E-04**	**1.29E-04**	**1.35E-04**	**9.67E-07**
$f_8(x)$	SOA	189.752579	251.8700343	0	329.110684	120.3292
	ESO	**1.7524E-06**	**1.90811E-06**	**0**	**3.41431E-06**	**1.06E-06**
$f_9(x)$	SOA	9968.755	9971.006	9178.597	10674.94	410.2554
	ESO	**8680.08**	**8694.393**	**7978.659**	**9087.25**	**292.4701**
$f_{10}(x)$	SOA	3.574E-16	-5.89E-16	-5.89E-16	2.96E-15	1.59E-15
	ESO	**3.397E-18**	**-5.887E-16**	**-5.887E-16**	**2.963E-15**	**1.34E-15**
$f_{11}(x)$	SOA	0.068656912	0	0	1.030401861	0.261282
	ESO	**4.07082E-17**	**0**	**0**	**1.22125E-15**	**2.22E-16**
$f_{12}(x)$	SOA	1.50709	1.656081	0.637	1.668971	0.270905
	ESO	**0.053166**	**0.03205**	**0.00301**	**0.185242**	**0.048696**
$f_{13}(x)$	SOA	14.24916	17.88704	5.798664	25.05247	6.987106
	ESO	**1.836966**	**1.458072**	**0.259541**	**5.8**	**1.584617**

Table 5: Comparison for ESO on standard benchmark functions

Function	Function	PSO [63]	GA [63]	DE [63]	HHO [63]
$f_1(x)$	Mean	1.83E+04	1.03E+03	1.33E−03	4.24E-287
	StDev	3.01E+03	5.79E+02	5.92E−04	0.00E+00
$f_2(x)$	Mean	3.58E+02	2.47E+01	6.83E−03	1.72E-159
	StDev	1.35E+03	5.68E+00	2.06E−03	3.35E-170
$f_3(x)$	Mean	4.05E+04	2.65E+04	3.97E+04	3.03E-289
	StDev	8.21E+03	3.44E+03	5.37E+03	0.00E+00
$f_4(x)$	Mean	4.39E+01	5.17E+01	1.15E+01	3.19E-135
	StDev	3.64E+00	1.05E+01	2.37E+00	2.23E-134
$f_5(x)$	Mean	1.96E+07	1.95E+04	1.06E+02	2.84E+01
	StDev	6.25E+06	1.31E+04	1.01E+02	1.80E-01
$f_6(x)$	Mean	1.87E+04	9.01E+02	1.44E−03	0.00E+00
	StDev	2.92E+03	2.84E+02	5.38E−04	0.00E+00

$f_7(x)$	Mean	1.07E+01	1.91E−01	5.24E−02	2.29E-04
	StDev	3.05E+00	1.50E−01	1.37E−02	1.35E-04
$f_8(x)$	Mean	−3.86E+03	−1.26E+04	−6.82E+03	−1.17E+04
	StDev	2.49E+02	4.51E+00	3.94E+02	1.46E+03
$f_9(x)$	Mean	2.87E+02	9.04E+00	1.58E+02	0.00E+00
	StDev	1.95E+01	4.58E+00	1.17E+01	0.00E+00
$f_{10}(x)$	Mean	1.75E+01	1.36E+01	1.21E−02	5.89E-16
	StDev	3.67E−01	1.51E+00	3.30E−03	2.96E-31
$f_{11}(x)$	Mean	1.70E+02	1.01E+01	3.52E−02	0.00E+00
	StDev	3.17E+01	2.43E+00	7.20E−02	0.00E+00
$f_{12}(x)$	Mean	1.51E+07	4.77E+00	2.25E−03	1.83E-03
	StDev	9.88E+06	1.56E+00	1.70E−03	4.50E-04
$f_{13}(x)$	Mean	5.73E+07	1.52E+01	9.12E−03	3.48E-01
	StDev	2.68E+07	4.52E+00	1.16E−02	2.46E-01

Table 5: Comparison for ESO on standard benchmark functions

Function	Function	BBO [63]	SOA	ESO
$f_1(x)$	Mean	7.59E+01	8.26E-297	**7.78E-297**
	StDev	2.75E+01	0.00E+00	**0.00E+00**
$f_2(x)$	Mean	1.36E−03	4.68E-149	**4.55E-149**
	StDev	7.45E−03	4.84E-150	**4.90E-150**
$f_3(x)$	Mean	1.21E+04	1.13E-297	**1.10E-297**
	StDev	2.69E+03	0.00E+00	**0.00E+00**
$f_4(x)$	Mean	3.02E+01	2.96E-150	**2.89E-150**
	StDev	4.39E+00	1.64E-151	**1.65E-151**
$f_5(x)$	Mean	1.82E+03	2.90E+01	**2.87E+01**
	StDev	9.40E+02	1.02E-02	**7.00E-02**
$f_6(x)$	Mean	6.71E+01	0.00E+00	**0.00E+00**
	StDev	2.20E+01	0.00E+00	**0.00E+00**
$f_7(x)$	Mean	2.91E−03	1.73E-04	**1.30E-04**
	StDev	1.83E−03	1.98E-05	**9.67E-07**
$f_8(x)$	Mean	−1.24E+04	-1.90E+02	**1.75E-06**
	StDev	3.50E+01	1.20E+02	**1.07E-06**
$f_9(x)$	Mean	0.00E+00	9.97E+03	**8.68E+03**
	StDev	0.00E+00	4.10E+02	**2.92E+02**
$f_{10}(x)$	Mean	2.13E+00	3.57E-16	**3.40E-18**
	StDev	3.53E−01	1.60E-15	**1.35E-15**
$f_{11}(x)$	Mean	1.46E+00	6.87E-02	**4.07E-17**
	StDev	1.69E−01	2.61E-01	**2.23E-16**
$f_{12}(x)$	Mean	6.68E−01	1.51E+00	**5.32E-02**
	StDev	2.62E−01	2.71E-01	**4.87E-02**
$f_{13}(x)$	Mean	1.82E+00	1.42E+01	**1.84E+00**
	StDev	3.41E−01	6.99E+00	**1.58E+00**

The convergence curves using logarithmic scale for standard benchmark optimization problems are given in Figure 1, and these curves clearly show that the ESO converges to its optimal value faster than SOA. For the functions ($f_1 - f_7$), f_{12}-f_{13} ESO converges in less than 20 iterations and shows the same trend as f_1 converges. For the other functions, the convergence curves are given and shows that ESO has faster convergence than SOA.

(i) Function,f_1

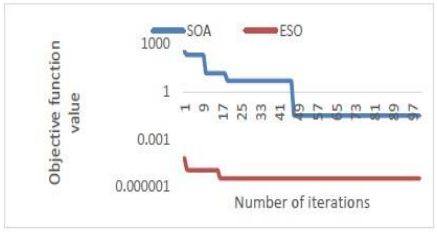

(ii) Function,f_8

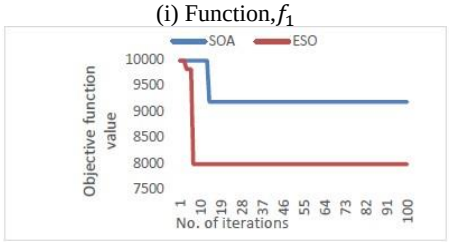

(iii) Function,f_9

(iv) Function,f_{10}

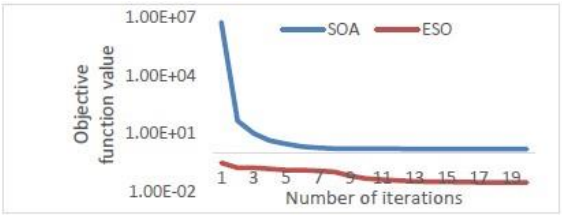

(v) Function,f_{11}

Figure 1: Convergence curves of standard benchmark problems

A whisker-box plot for the standard benchmark optimization problem is given in Figure 2. Box plots show that ESO performs better than SOA because of having small quartiles and less number of outliers. For the functions f_2, f_7, f_{11} and f_{12} SOA has more outliers than ESO. Function f_8, f_{10} and f_{13} has a large quartile of SOA compared to ESO. This depicts that the ESO gives competing results over the SOA for this function. For functions f_1, $f_3 - f_6$ *and* f_9 SOA has a higher median value than ESO; hence, ESO gives better results for all the functions.

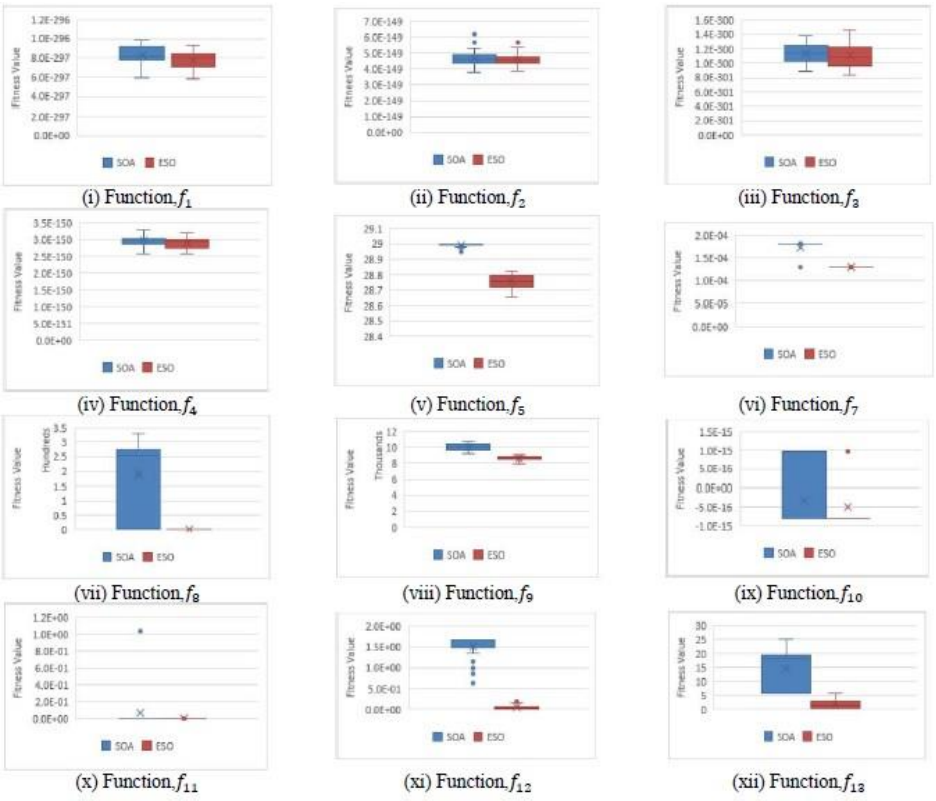

Figure 2: Whiskers Box plot curves for standard benchmark functions

6.2. Hydrothermal test systems

The proposed emended snake optimization approach has been implemented to solve two real-world complex engineering problems. The two practical problems are taken from the power system generation scheduling background. This paper addresses the HEGS problem using the proposed ESO. In HEGS problems, the variable head is considered. TS1 and TS2 denote the power system test problems. The description of these test systems along with parameters, is given in Table 8. In the proposed ESO, 30 independent trial runs while implementing ESO. The operating fuel cost of thermal units is $/hr. A detailed discussion of results obtained by ESO is given in the ensuing subsections. The detail of the systems undertaken for the study is given in Table 6.

Table 6: Elements of test systems taken for study

Test System	Time Horizon	Number of Thermal Generators	Number of Hydro Generators	Number of Pumped Storage Generators	Number of Solar Generators	Total Generating Units	Reference
TS1	24h	2	2	1	1	6	[64]
TS2	24h	5	4	1	1	11	

The study uses two electric power test systems with four different cases to validate the proposed method for solving the HEGS problem. The time horizon is set at 24 hours, then divided into 24-time intervals. Each period lasts for one hour.
Four cases (Case-I, II, III, and IV) are taken in the study and are represented in Table 7 for the test system TS1. In Case-I, hydrothermal units, pumped storage units, and solar units are all considered in the multiobjective framework. In Case-II, the effect of pumped storage units is considered. In Case-III, hydrothermal units with multi objectives framework are considered while not considering the pumped storage and wind units. Case-IV considers only hydrothermal units with a single objective while not considering pumped storage units and solar units.

Table 7: Different cases of the test system taken for experimental studies

Test System	Cases	Hydrothermal	Pumped Storage	Solar	Number Of Objectives
TS1	Case-I	✓	✓	✓	Two
	Case-II	✓	✓	×	Two
	Case-III	✓	×	×	Two
	Case-IV	✓	×	×	Single

The pumped storage hydro unit's data for the test system is given in Table 8, representing the generation and pumping coefficients along with power generation limits of pumped storage hydro generators.

Table 8: Pumped storage unit input data

Pumped Storage Unit	Generation Coefficients			Pumping Coefficients			P_i^{min} (MW)	P_i^{max} (MW)
	χ_l^+ (m^3/MW^2h)	ξ_l^+ (m^3/MWh)	φ_l^+ (m^3/h)	χ_l^- (m^3/MW^2h)	ξ_l^- (m^3/MWh)	φ_l^- (m^3/h)		
TS1	0.00022	0.306	1.98	0.00036	0.612	0.936	0	300

The gaseous pollutants emission coefficients of the thermal station for test systems TS1 and TS2 are given in Table 9 and Table 10, respectively.

Table 9: Emission coefficients for hydrothermal test system TS1

Thermal Unit	a_{2i} (lb/MW^2h)	b_{2i} (lb/MWh)	c_{2i} (lb/h)	d_{2i} (lb/h)	e_{2i} (MW^{-1})
1	0.00232	3.84632	182.2605	0.0	0.0
2	0.00232	3.84632	182.2605	0.0	0.0

Table 10: Emission coefficients for hydrothermal test system TS2

Thermal Unit	a_{2i} (lb/MW^2h)	b_{2i} (lb/MWh)	c_{2i} (lb/h)	d_{2i} (lb/h)	e_{2i} (MW^{-1})
1	0.00419	0.32767	13.85932	0.0	0.0
2	0.00419	0.32767	13.85932	0.0	0.0
3	0.00683	0.54551	40.2669	0.0	0.0
4	0.00683	0.54551	40.2669	0.0	0.0
5	0.00461	0.51116	42.89553	0.0	0.0

Test System-TS1: the first hydrothermal test system TS1 considers the two thermal, two hydro, one pumped storage, and one solar unit for power generation for 24 hours [64].
Case-I: The solar commitment table for the electric power test system TS1 is given in Table 11. When U_{tk}^{S} is set to 0, which means the solar unit is OFF, and if U_{tk}^{S} is set 1 presents a particular solar unit is ON for the respective interval.

Table 11: Commitment schedule of solar units for test System-TS1(Case-I)

Interval, t	Solar committed units (U_{tk}^{S})	Interval, t	Solar committed units (U_{tk}^{S})
1	0000000000000	13	0111110011111
2	0000000000000	14	1111111110101
3	0000000000000	15	0011111011111
4	0000000000000	16	0000000000000
5	0000000000000	17	0000000000000
6	0000000000000	18	0000000000000
7	0000000000000	19	0000000000000
8	0000000000000	20	0000000000000
9	0000000000000	21	0000000000000
10	1111011111110	22	0000000000000
11	1100111111111	23	0000000000000
12	1111110111111	24	0000000000000

The power generation schedules for total thermal, total hydro, pumped storage and solar units are shown in Table 12. Total demand and transmission losses, along with power mismatch, are also included in Table 12. The power generation schedule of thermal and hydro generating units is given in Table 13. The solar power generation schedule is given in Table 14. The water discharge rates for hydro units are shown in Table 15. The lowest obtained thermal fuel cost is 54780.5 $/hr, while the emission is 76029.75 tons for 24 hours. The power balance equality constraint $|E_t^{PD}|$ in Tables 12 and 15 is less than 0.001, and the volume constraint $\left|E_j^{v}\right|$ is nearly 0. The solutions are practical because both the power balance equality and volume constraints are met.

Table 12: Power generation, load demand, and transmission losses for test System-TS1(Case-I)

Interval, t	P_{Dt} (MW)	P_{Lt} (MW)	Total thermal generation (MW)	Total hydro generation (MW)	Pumped storage generation (MW)	**Solar generation (MW)**	$\boldsymbol{\lvert E_t^{PD}\rvert}$ **(MW)**
1	800	28.9527	500.9984	424.66232	-96.70743	0	0.00059
2	700	20.32185	297.1892	435.88093	-12.74733	0	0.00095
3	600	13.62555	315.6852	314.75965	-16.81863	0	0.00067
4	600	15.94972	385.28521	305.7048	-75.03928	0	0.00101
5	600	19.76236	321.7459	406.60673	-108.5894	0	0.00087
6	650	20.72585	393.5619	376.17342	-99.00908	0	0.00039
7	800	24.47142	459.4611	393.9913	-28.98009	0	0.00089
8	1000	41.55117	643.9629	467.3848	-69.79615	0	0.00038
9	1330	41.51477	690.0295	432.62016	248.866	0	0.00089
10	1350	38.63902	593.938	474.2594	-70.04523	390.4879	0.00105
11	1450	53.00381	499.5139	685.5355	-81.40521	399.3604	0.00078
12	1500	46.84646	634.0257	540.5567	-6.799764	379.0646	0.00078
13	1300	55.07063	616.5907	638.686	-79.04504	178.8361	0.00287
14	1350	34.91125	584.6223	432.60733	-31.60393	399.2863	0.00075
15	1350	35.3909	638.9941	397.08589	-56.47545	405.7871	0.00074
16	1370	41.81533	649.7686	462.0473	300	0	0.00057

17	1450	47.54082	733.1277	464.41412	300	0	0.001
18	1570	59.2019	922.2797	406.92335	299.9997	0	0.00085
19	1430	45.55378	728.7493	447.2484	299.5569	0	0.00082
20	1350	41.01181	666.0114	445.46108	279.5401	0	0.00077
21	1270	62.44126	743.5905	615.6918	-26.84037	0	0.00067
22	1150	55.02782	892.5554	365.75297	-53.27977	0	0.00078
23	1000	37.26646	688.8693	360.8993	-12.50165	0	0.00049
24	900	34.65259	669.8767	328.68553	-63.90866	0	0.00098
					Minimum Fuel Cost ($)	**54780.5**	
					Emission (ton)	**76029.75**	

Table 13: Power generation schedule of thermal and hydro generating units for test System-TS1(Case-I)

Interval, t	P_{1t} (MW)	P_{2t} (MW)	P_{3t} (MW)	P_{4t} (MW)
1	168.3542	332.6442	374.361	50.30132
2	122.1892	175	342.7471	93.13383
3	95	220.6852	309.5984	5.16125
4	97.32411	287.9611	199.0343	106.6705
5	146.7459	175	307.2339	99.37283
6	158.0596	235.5023	316.3407	59.83272
7	138.5148	320.9463	368.9857	25.0056
8	107.6718	536.2911	358.6882	108.6966
9	179.0761	510.9534	371.3794	61.24076
10	205.5618	388.3762	291.4461	182.8133
11	224.557	274.9569	484.6985	200.837
12	103.931	530.0947	432.6949	107.8618
13	218.0451	398.5456	389.0502	249.6358
14	212.4805	372.1418	415.3465	17.26083
15	184.8013	454.1928	360.8466	36.23929
16	119.1722	530.5964	213.1019	248.9454
17	232.8556	500.2721	400.4961	63.91802
18	243.5658	678.7139	322.6775	84.24585
19	187.0096	541.7397	385.61	61.6384
20	211.7625	454.2489	362.9722	82.48888
21	250.2344	493.3561	435.5349	180.1569
22	336.3335	556.2219	342.7419	23.01107
23	245.1539	443.7154	251.5762	109.3231
24	268.8951	400.9816	244.8358	83.84973

Table 14: Solar power generation for test System-TS1(Case-I)

Interval, t	Solar power generation (MW)												
	S_{1t}	S_{2t}	S_{3t}	S_{4t}	S_{5t}	S_{6t}	S_{7t}	S_{8t}	S_{9t}	S_{10t}	S_{11t}	S_{12t}	S_{13t}
1	0	0	0	0	0	0	0	0	0	0	0	0	0
2	0	0	0	0	0	0	0	0	0	0	0	0	0
3	0	0	0	0	0	0	0	0	0	0	0	0	0
4	0	0	0	0	0	0	0	0	0	0	0	0	0
5	0	0	0	0	0	0	0	0	0	0	0	0	0
6	0	0	0	0	0	0	0	0	0	0	0	0	0
7	0	0	0	0	0	0	0	0	0	0	0	0	0
8	0	0	0	0	0	0	0	0	0	0	0	0	0
9	0	0	0	0	0	0	0	0	0	0	0	0	0
10	22.64	28.30	28.30	28.30	0.00	33.96	39.61	39.61	45.27	45.27	45.27	45.27	0.00
11	22.82	28.53	0.00	0.00	34.23	34.23	39.94	39.94	45.64	45.64	45.64	45.64	45.64
12	22.97	28.72	28.72	28.72	34.46	34.46	0.00	40.20	45.95	45.95	45.95	45.95	45.95
13	0.00	28.84	28.84	28.84	34.61	34.61	0.00	0.00	46.15	46.15	46.15	46.15	46.15
14	23.15	28.93	28.93	28.93	34.72	34.72	40.51	40.51	46.29	0.00	46.29	0.00	46.29
15	0.00	0.00	28.98	28.98	34.78	34.78	40.58	0.00	46.38	46.38	46.38	46.38	46.38
16	0	0	0	0	0	0	0	0	0	0	0	0	0
17	0	0	0	0	0	0	0	0	0	0	0	0	0
18	0	0	0	0	0	0	0	0	0	0	0	0	0
19	0	0	0	0	0	0	0	0	0	0	0	0	0
20	0	0	0	0	0	0	0	0	0	0	0	0	0
21	0	0	0	0	0	0	0	0	0	0	0	0	0
22	0	0	0	0	0	0	0	0	0	0	0	0	0
23	0	0	0	0	0	0	0	0	0	0	0	0	0
24	0	0	0	0	0	0	0	0	0	0	0	0	0

Table 15: Hydro units water discharge for test System-TS1(Case-I)

Interval, t	Q_{1t} (m^3/h)	Q_{2t} (m^3/h)	Q_{3t} (m^3/h)	Interval, t	Q_{1t} (m^3/h)	Q_{2t} (m^3/h)	Q_{3t} (m^3/h)
1	130.5216	51.39428	-63.4878	13	136.096	273.6637	-51.5609
2	117.3569	96.10519	-8.79586	14	147.3295	17.97396	-20.6372
3	103.9892	6.45289	-11.3308	15	124.1571	36.51846	-36.6472
4	62.61987	110.5428	-48.8872	16	67.28139	271.7531	113.22
5	102.998	102.5355	-71.6377	17	140.7599	64.05476	113.22
6	106.5685	60.91014	-65.0586	18	108.5427	84.85336	113.2198
7	127.9982	25.7999	-18.9742	19	134.3148	61.63469	113.027
8	123.6619	112.3376	-45.405	20	124.7987	82.88915	104.3981
9	128.892	62.21019	91.51082	21	155.745	188.8869	-17.6217
10	96.63136	195.1728	-45.57	22	116.4072	23.32771	-34.5652
11	178.6792	215.8065	-53.1416	23	81.03925	110.6221	-8.64327
12	155.0772	110.6622	-5.1141	24	78.53374	83.89132	-41.5185
Computed Volume (m^3)					**2849.999**	**2449.999**	
Available Volume V_j (m^3)					**2850**	**2450**	
Error in Volume $\lvert E_j^v \rvert$ (m^3)					**0.001**	**0.001**	

The variation of power generation schedules for thermal and hydro units for all four cases is given in Figure 3- Figure 6 for the sake of comparison. Whisker box plots for hydrothermal for all cases of test system TS1 of SOA and ESO are shown in Figure 7. Box plot for TS1 (Case-I-Case-III) shows that SOA has a higher median value than ESO. For

test system TS1 (case-IV), SOA has a larger quartile than ESO, which shows that ESO gives better results than SOA and performs better.

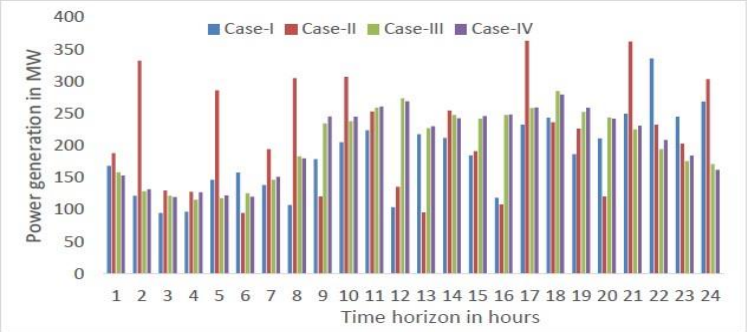

Figure 3: Power generation schedule for thermal unit 1 $\boldsymbol{P_{1t}}$ (MW) for all cases of TS1

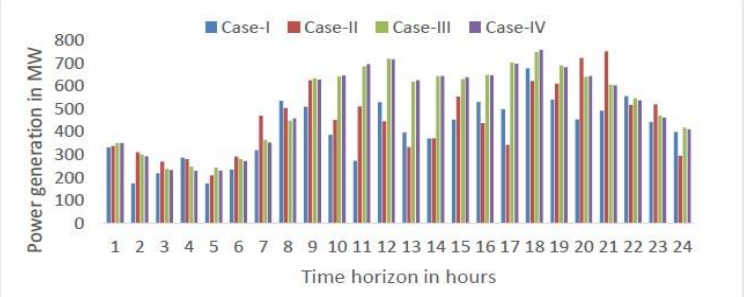

Figure 4: Power generation schedule for thermal unit 2 P_{2t} (MW) for all cases of TS1

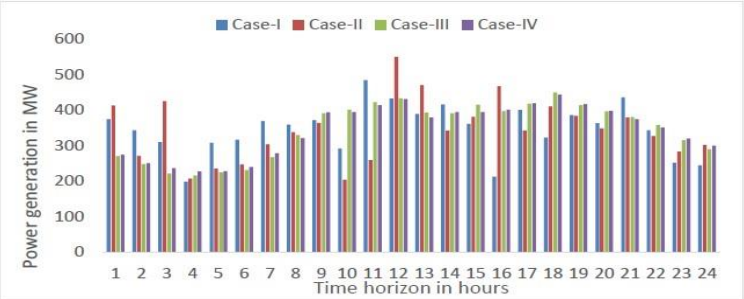

Figure 5: Power generation schedule for hydro unit 1 P_{3t} (MW) for all cases of TS1

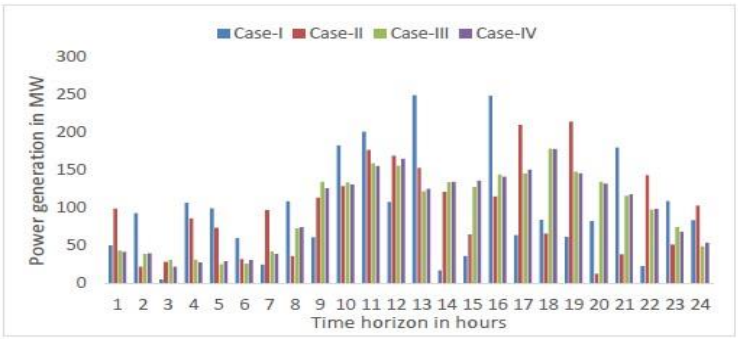

Figure 6: Power generation schedule for hydro unit 2 P_{4t} (MW) for all cases of TS1

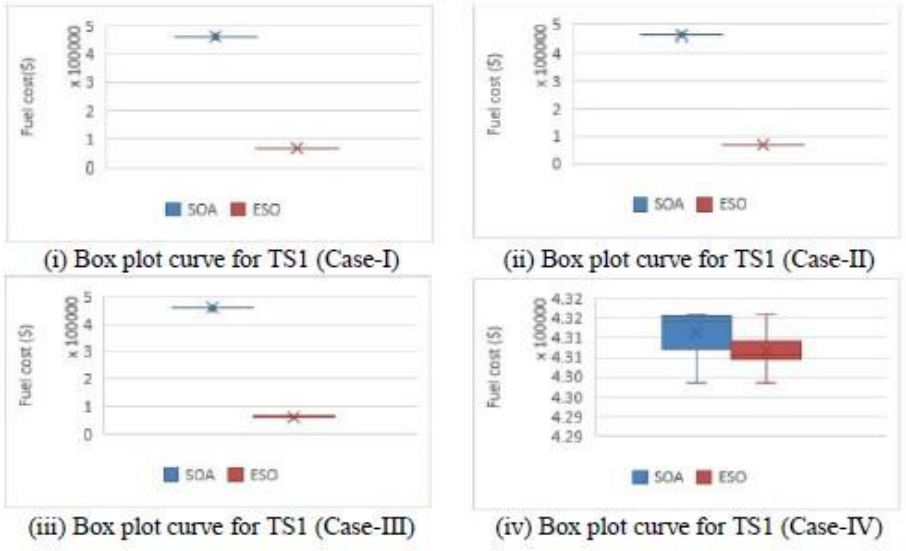

Figure 7: Whisker box plots for all cases of TS1

The convergence behaviour of SOA and ESO is depicted in Figure 8. These curves show that ESO converges faster than SOA to its optimal value in all cases. Table 16 shows the Commitment schedule of solar units for the System-TS2 (Case-I) electric power test system. When U_{tk}^{S} is set to 0, the specific solar unit is turned off, and when U_{tk}^{S} is set to 1, the specific solar unit is turned on during the specified interval.

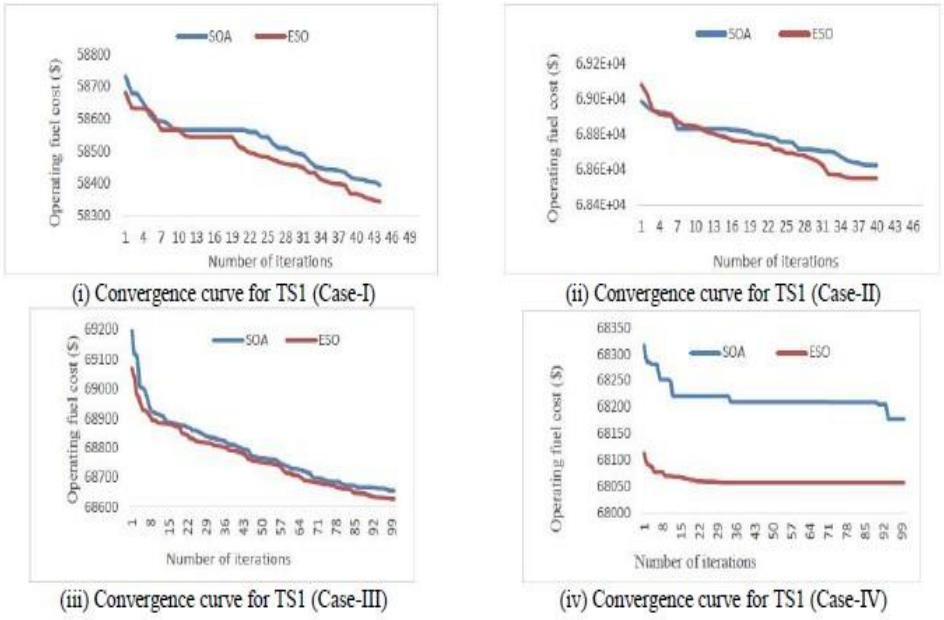

Figure 8: Convergence curves for all cases of TS1

Table 16: Commitment schedule of solar units for test System-TS2

Interval, t	Solar committed units (U_{tk}^{S})	Interval, k	Solar committed units (U_{tk}^{S})
1	0000000000000	13	1111111111111
2	0000000000000	14	1111111111111
3	0000000000000	15	1111111111111
4	0000000000000	16	0000000000000
5	0000000000000	17	0000000000000
6	0000000000000	18	0000000000000
7	0000000000000	19	0000000000000
8	0000000000000	20	0000000000000
9	0000000000000	21	0000000000000
10	1111111111111	22	0000000000000
11	1111111111111	23	0000000000000
12	1111111111111	24	0000000000000

Table 17 shows the power generation schedules for total thermal, total hydro, pumped storage, and solar units. Table 17 additionally includes total demand and transmission losses along with power mismatch.

Table 17: Power generation, load demand, and transmission losses for test System-TS2

Interval, t	P_{Dt} (MW)	P_{Lt} (MW)	Total thermal generation (MW)	Total hydro generation (MW)	Pumped storage generation (MW)	Solar generation (MW)	$\lvert E_t^{PD} \rvert$ (MW)
1	5448	595.8401	3925.959	2031.02	86.86116	0	4.40E-04
2	5776	689.1898	4305.402	2025.886	133.902	0	5.00E-04
3	5664	642.9438	4055.547	2118.866	132.5305	0	1.20E-03
4	5624	650.1658	4097.733	2043.935	132.4978	0	9.00E-04
5	5928	732.8257	4451.639	2122.711	86.47606	0	3.40E-04
6	6064	749.3846	4377.121	2302.566	133.6969	0	8.00E-04
7	6068	776.1031	4582.673	2176.518	84.91042	0	1.18E-03
8	5856	711.7569	4381.968	2087.207	98.58076	0	1.04E-03
9	5480	629.9535	4156.435	1830.837	122.681	0	8.00E-04
10	5464	526.8383	3638.912	1954.015	-83.1257	481.0357	1.21E-03
11	5728	534.4049	3685.643	1958.276	133.5471	484.9376	5.00E-04
12	5536	488.8742	3356.733	2126.505	53.44678	488.1893	4.20E-04
13	5400	495.3604	3541.16	1920.044	-56.201	490.3569	5.80E-04
14	5828	559.6325	3813.344	1951.188	131.2252	491.8744	9.00E-04
15	3928	227.6189	2271.328	1477.872	-86.3232	492.7415	2.40E-04
16	3840	276.225	2486.462	1635.857	-6.09418	0	7.81E-04
17	3784	270.683	2387.853	1721.542	-54.7127	0	8.70E-04
18	3608	253.0855	2471.499	1476.077	-86.4915	0	6.70E-04
19	3584	236.6901	2303.97	1526.932	-10.2127	0	9.50E-04
20	3544	233.5538	2346.959	1434.979	-4.38481	0	1.31E-03
21	3528	234.4278	2233.638	1591.308	-62.5184	0	3.40E-04
22	3552	247.3346	2426.07	1455.834	-82.569	0	5.80E-04
23	3688	274.8646	2553.768	1496.872	-87.7768	0	9.60E-04
24	3840	288.6955	2508.892	1708.058	-88.2547	0	1.70E-04
					Minimum Fuel Cost($)		**429842.8**
					Emission(ton)		**375341.9**

Table 18 shows the solar power generation schedule. Table 19 shows the water discharge rates for hydro units. The lowest fuel cost obtained is 429842.8 $/h, while the emission is 375341.9 tons. The power balance equality constraint $|E_t^{PD}|$ is less than 1.31E-03, and the volume constraint $|E_j^v|$ is nearly 0. The solutions are practical since they satisfy both the power balance equality and volume constraints.

Table 18: Solar power generation for test System-TS2(Case-I)

Interval, t	Solar power generation (MW)												
	S_{1t}	S_{2t}	S_{3t}	S_{4t}	S_{5t}	S_{6t}	S_{7t}	S_{8t}	S_{9t}	S_{10t}	S_{11t}	S_{12t}	S_{13t}
1	0	0	0	0	0	0	0	0	0	0	0	0	0
2	0	0	0	0	0	0	0	0	0	0	0	0	0
3	0	0	0	0	0	0	0	0	0	0	0	0	0
4	0	0	0	0	0	0	0	0	0	0	0	0	0
5	0	0	0	0	0	0	0	0	0	0	0	0	0
6	0	0	0	0	0	0	0	0	0	0	0	0	0
7	0	0	0	0	0	0	0	0	0	0	0	0	0
8	0	0	0	0	0	0	0	0	0	0	0	0	0
9	0	0	0	0	0	0	0	0	0	0	0	0	0
10	22.64	28.30	28.30	28.30	33.96	33.96	39.61	39.61	45.27	45.27	45.27	45.27	45.27

11	22.82	28.53	28.53	28.53	34.23	34.23	39.94	39.94	45.64	45.64	45.64	45.64	45.64
12	22.97	28.72	28.72	28.72	34.46	34.46	40.20	40.20	45.95	45.95	45.95	45.95	45.95
13	23.08	28.84	28.84	28.84	34.61	34.61	40.38	40.38	46.15	46.15	46.15	46.15	46.15
14	23.15	28.93	28.93	28.93	34.72	34.72	40.51	40.51	46.29	46.29	46.29	46.29	46.29
15	23.19	28.98	28.98	28.98	34.78	34.78	40.58	40.58	46.38	46.38	46.38	46.38	46.38
16	0	0	0	0	0	0	0	0	0	0	0	0	0
17	0	0	0	0	0	0	0	0	0	0	0	0	0
18	0	0	0	0	0	0	0	0	0	0	0	0	0
19	0	0	0	0	0	0	0	0	0	0	0	0	0
20	0	0	0	0	0	0	0	0	0	0	0	0	0
21	0	0	0	0	0	0	0	0	0	0	0	0	0
22	0	0	0	0	0	0	0	0	0	0	0	0	0
23	0	0	0	0	0	0	0	0	0	0	0	0	0
24	0	0	0	0	0	0	0	0	0	0	0	0	0

Table 19: Hydro units water discharge (m^3 / h) for test System-TS2

Interval, t	Q_{1t}	Q_{2t}	Q_{3t}	Q_{4t}	Q_{5t}
1	502.8061	379.1065	427.7679	425.1179	30.18921
2	491.0201	532.8895	344.3972	369.4405	46.82683
3	368.2838	457.3678	583.4129	441.4314	46.32823
4	451.8486	393.5674	335.1059	582.399	46.31636
5	499.9757	434.3516	469.2318	441.8903	30.05695
6	550.8453	542.0093	592.9739	400.0594	46.75223
7	443.775	560.3033	362.6369	558.8583	29.5199
8	396.0083	443.4529	498.2304	464.7943	34.24483
9	360.9429	413.8032	391.7292	330.3741	42.77131
10	523.4988	446.697	313.5406	368.1327	-54.2965
11	424.7621	405.4039	414.2517	398.9146	46.69775
12	442.3307	409.4978	581.0191	424.4908	18.95173
13	349.4112	512.1243	380.1193	364.8779	-36.4681
14	330.5711	463.199	387.6797	459.8254	45.85444
15	227.3089	270.0647	270.8375	352.9139	-56.4484
16	441.095	238.281	362.0494	255.6229	-4.67901
17	394.3742	314.267	378.6937	289.5381	-35.4978
18	273.2868	275.6919	303.5538	261.6299	-56.5619
19	293.6972	248.3217	260.1429	368.9933	-7.22369
20	345.5628	261.7812	195.2439	278.9991	-3.62642
21	252.7155	292.8867	365.6722	325.3212	-40.6044
22	191.6496	233.3528	388.5141	295.7505	-53.9226
23	276.1396	203.3854	193.7827	500.3016	-57.4291
24	343.0918	443.1964	374.4157	215.3243	-57.7519
Computed Volume (m^3)	**9175**	**9175.001**	**9175**	**9175.001**	
Available Volume V_j (m^3)	**9175.0**	**9175.0**	**9175.0**	**9175.0**	
Error in Volume $\lvert E_j^v \rvert$ (m^3)	**0.00E+00**	**9.77E-04**	**0.00E+00**	**9.77E-04**	

Whisker box plots for all cases of the test system are given in Figure 9. For TS2 (Case-I), SOA has two outliers, and ESO has one outlier. SOA has a higher median value than ESO, which depicts that ESO gives better results than SOA and performs better. For TS2 (Case-II-Case-IV), SOA has a higher median value than ESO, which shows that ESO performs better and gives better results than SOA.

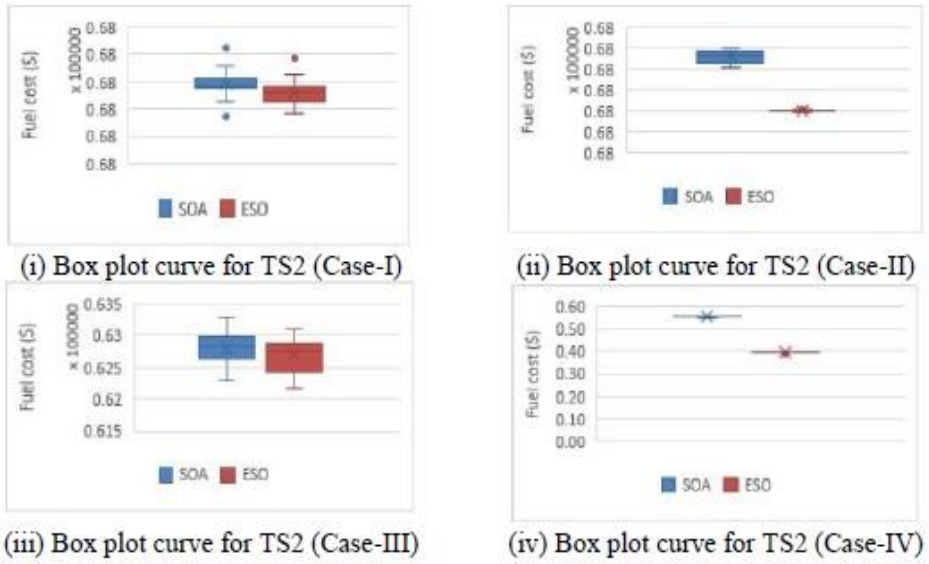

Figure 9: Whisker box plots for all cases of TS2

The convergence curves for all cases of TS2 are given in Figure 10. The convergence plots show that ESO converges faster than SOA to its optimal value. The results for solving electric test system TS1 using the proposed ESO in terms of emission and operating cost (minimum, average, maximum, and standard deviation) are compared with predator-prey optimization (PPO), and SOA is given in Table 20.

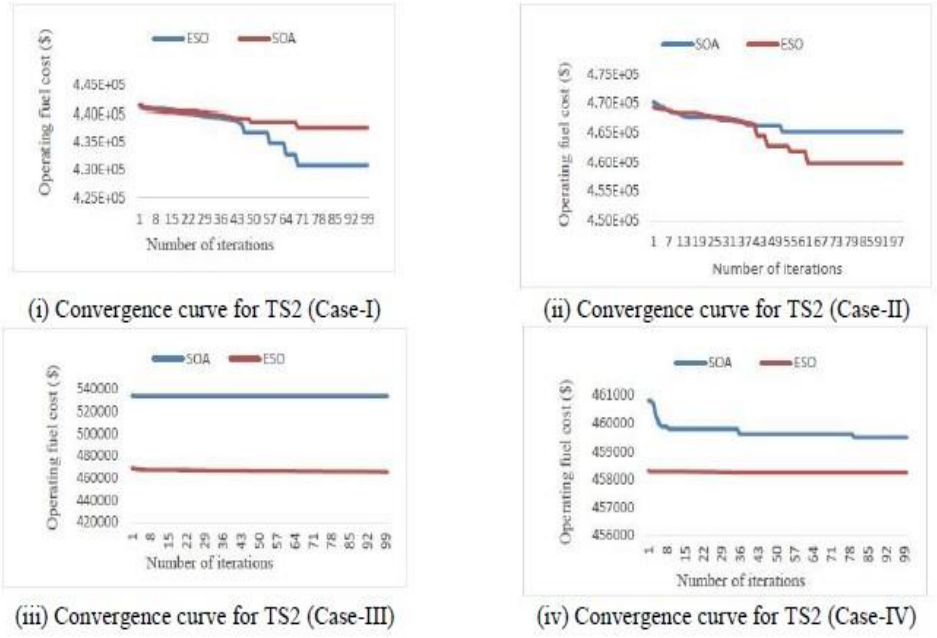

Figure 10: Convergence curves for all cases of TS2

It is observed that ESO obtains the minimum operating cost in every case (Case-I – Case-IV) for TS1. In Case-IV of TS1, there is one objective, but if emission is calculated as per the thermal power generation schedule, it comes out to be 94946.71. The results show that in Case-III, TS1, the emission (ton) is decreased from 94946.71 to 94934.42, offering a significant drop of 0.0129%, but the operating cost is increased due to the conflicting nature of objectives considered. In Case-II, TS1, the emission (ton) drops from 94934.42 to 85709.63, showing a percentage drop of 9.717%, and fuel cost ($/h) is reduced from 67995.88 to 62171.95, showing a cost reduction of 8.565%, due to penetration of pumped storage units. Similarly, in Case-I, TS1 gives the least emission and fuel cost due to the penetration of pumped storage and solar units. The emission (ton) is reduced from 85709.63 to 76029.75, offering a significant drop of 11.29%, and operating fuel cost ($/hr) is reduced from 62171.95 to 54780.5 showing an 11.88% reduction in operating cost.

Table 20: Comparison of results (emission, thermal operating cost, solar cost and total cost) for test system TS1

Test System		Case-IV			Case-III		Case-II		Case-I	
Method		PPO	SOA	**ESO**	SOA	**ESO**	SOA	**ESO**	SOA	**ESO**
Emission		NA	94946.7	**94946.7**	94969.6	**94934.4**	86537.2	**85709.6**	76029.7	**76029.7**
Thermal operating cost	Min	68379.7	67989.7	**67989.7**	68220.3	**67995.8**	62429.4	**62171.9**	54780.5	**54780.5**
	Avg	NA	67996.9	**67992.9**	68261.7	**68000.9**	62802.1	**62744.1**	55217.6	**55170.6**
	Max	NA	68002.2	**67999.3**	68304.2	**68010.3**	63302.2	**63096.7**	55409.5	**55697.7**
	SD	NA	3.5493	**3.4549**	30.1311	**3.32653**	310.657	**251.658**	112.470	**192.946**
Solar cost($/hr)		–	–	–	–	–	–	–	642337.2	**642337.2**
Total cost($/hr)		–	–	–	–	–	–	–	697117.7	**697117.7**

The results for solving electric test system TS2 using the proposed ESO in terms of emission and operating cost (minimum, average, maximum, and standard deviation) are compared with real coded genetic algorithm (RCGA) [65], PPO [64], and SOA are given in Table 21. It is observed that ESO obtains the minimum operating cost in each case (Case-I – Case-IV) for TS2. In Case-IV of TS2, since there is one objective if emission (ton) is calculated as per the thermal power generation schedule, it comes out to be 479875. The results show that in Case-III, TS2, the emission (ton) is decreased from 479875 to 401783.4, offering a significant drop of 16.27%, but the operating cost is increased due to the conflicting nature of objectives considered. In Case-II, TS2, operating fuel cost ($/hr) is reduced from 458337.8 to 456229, showing a cost reduction of 0.46% due to penetration of pumped storage units. The emission increased by 0.19%. Similarly, in Case-I, TS2 gives the least emission and fuel cost due to the penetration of pumped storage and solar units. The emission (ton) is reduced from 402578.6 to 375341.9, offering a significant drop of 6.765%, and operating fuel cost ($/hr) is reduced from 456229 to 429842.8 showing a 5.783% reduction in operating cost.

Table 21: Comparison of results (emission, thermal operating cost, solar cost, and total cost) for test system TS1

Case	Method	Emission	Thermal Operating cost ($/hr)				Solar cost($/hr)	Total cost($/hr)
			Min	Avg	Max	SD		
Case-I	SOA	375341.9	429842.8	431138.3	431584.9	566.9106	761919.8	1191762.6
	ESO	**375341.9**	**429842.8**	**431138.3**	**431584.9**	**566.9106**	761919.8	1191762.6
Case-II	SOA	406716.8	458868.1	458467.6	459731.5	885.4777	–	458868.1
	ESO	**402578.6**	**456229**	**458467.6**	**459731.5**	**885.4777**	–	**456229**
Case-III	SOA	412974.5	464352.1	464637.6	465027.2	204.3919	–	464352.1
	ESO	**401783.4**	**458337.8**	**458371.4**	**458473.7**	**28.39035**	–	**458337.8**
Case-IV	RCGA[65]	NA	461717.73	NA	NA	NA	–	461717.73
	PPO[64]	NA	458409.7	NA	NA	NA	–	458409.7
	SOA	684647.5	458181.2	458192.8	458206.2	7.367465	–	458181.2
	ESO	**479875**	**458176.7**	**458189.9**	**458192.8**	**6.747369**	–	**458176.7**

6.3. Statistical analysis

The Wilcoxon signed-rank test is applied on standard benchmark functions for result analysis and is given in Table 22. The Wilcoxon signed-rank test is a non-parametric test that compares two matched samples based on their ranks. The Wilcoxon signed-rank test is used for making inferences in paired-sample data concerning the value of the median of the population of differences. The results obtained by SOA are compared with the results obtained by ESO while solving the hydrothermal generation scheduling problem.

Table 22: Wilcoxon signed rank test ESO versus SOA for benchmark functions

Function	p-value	Function	p-value
f_1	1.087 E-04	f_8	5.1239E-04
f_2	6.147E-10	f_9	3.0104E-11
f_3	3.328E-05	f_{10}	8.0834E-05
f_4	1.668E-11	f_{12}	3.0104E-11
f_5	6.6363E-11	f_{13}	8.3695E-11
f_7	2.0519E-10		

Table 23 shows that the p-value obtained for every benchmark function is significant for 5%, which concludes that the proposed ESO method gives improved results for every benchmark function under consideration. This justifies the robustness of ESO.

Friedman's test is performed to obtain the mean ranking of all competing algorithms on ($f_1 - f_{13}$) benchmark optimization problems and proposed ESO. Figure 11 shows that the ESO obtains first rank having the mean rank value of 3.5 among all competing algorithms.

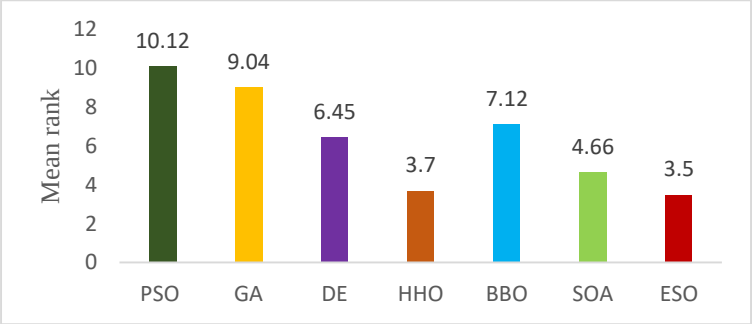

Figure 11: Mean ranking values of all competing algoritms and ESO on ($f_1 - f_{13}$) benchmark functions

Wilcoxon sign rank test is performed on test systems TS1 and TS2, and p-values for test systems are tabulated in Table 23, which shows that for both test systems, in all cases, p-values are significant for 5%, and this justifies that the results are statistically significant and ESO is a robust algorithm.

Table 23: Wilcoxon signed-rank test ESO versus SOA for test system TS1 and TS2

Test Systems	Case	p-value
TS1	Case-I	2.3890E-11
	Case-II	0.03844
	Case-III	3.0199E-11
	Case-IV	1.7E-03
TS2	Case-I	2.3E-03
	Case-II	1.5415E-10
	Case-III	3.0199E-11
	Case-IV	3.0199E-11

7. CONCLUSIONS

This paper proposes an emended snake optimizer (ESO) to address the multiobjective hybrid energy generation scheduling (HEGS) problem. A snake optimization algorithm is amended with simplex search method and opposition-based learning to enhance the snake optimizer's exploration and exploitation ability and convergence rate. The amendment improves the performance of SOA by enhancing the global solution accuracy, avoiding stagnation of local solutions and avoiding premature convergence. The proposed ESO technique is tested on thirteen standard benchmark problems. The results show that ESO gives better results during experimentation. The efficacy of the ESO is proved by the better convergence behavior while solving these standard benchmark problems. The competitive results obtained on standard benchmark problems prove the effectiveness of the ESO. To evaluate ESO's supremacy, two non-linear and highly constrained hydrothermal generation scheduling test systems are solved. An iterative repair technique is utilized to handle the equality constraints, and a replacement method is utilized to handle the inequality constraints. The proposed ESO significantly reduces the operating cost and emissions by 11.88% and 11.29%, respectively, for TS1. For TS2, the significant reduction in operating cost is 5.783%, and emission is 6.7765%. Box plots were given for the standard benchmark function to prove the robustness of ESO Whisker. Convergence curves are drawn to authenticate the results by a better convergence rate. Wilcoxon signed-rank test and Friedman rank test have been performed to justify the robustness of ESO.

The major limitation of renewable energy sources is the uncertainty due to fluctuations in weather conditions. which makes it difficult and challenging to predict and schedule their availability accurately. In the future, wind energy can be considered to enhance the scope of the present work. The optimal load flow considering demand side management can be the future scope study to apply the proposed ESO. A further modification is also possible in the proposed algorithm by hybridizing it with any other nature-inspired algorithm to achieve the improvement.

Funding: This research received no external funding.

REFERENCES

[1] A. J. Wood, B. F. Wollenberg, and G. B. Sheblé, "Power generation, operation, and control," *John Wiley & Sons*; 2013.

[2] C. A. Coello, G. T. Pulido, and M. S. Lechuga, "Handling multiple objectives with particle swarm optimization," *IEEE Transactions on Evolutionary Computation*, vol. 8, no. 3, pp. 256-79, 2004, https://doi.org/10.1109/TEVC.2004.826067.

[3] T. T. Anilkumar, S. P. Simon, and N. P. Padhy, "Residential electricity cost minimization model through open well-pico turbine pumped storage system," *Applied Energy*, vol. 194, pp. 23-35, 2017, https://doi.org/10.1016/j.apenergy.2017.03.020.

[4] M. Basu, "Fuel constrained short-term hydrothermal generation scheduling," *Energy*, vol. 239, pp. 122352, 2022, https://doi.org/10.1016/j.energy.2021.122352.

[5] J. I. Pérez-Díaz, and J. Jiménez, "Contribution of a pumped-storage hydropower plant to reduce the scheduling costs of an isolated power system with high wind power penetration," *Energy*, vol. 109, pp. 92-104, 2016, https://doi.org/10.1016/j.energy.2016.04.014.

[6] P. T. Ha, D.T.Tran, and T.T. Nguyen, "Electricity generation cost reduction for hydrothermal systems with the presence of pumped storage hydroelectric plants," *Neural Computing and Applications*, vol. 34, no. 12, pp. 9931-53, 2022, https://doi.org/10.1007/s00521-022-06977-0.

[7] K. Deb, "Optimization for engineering design: Algorithms and examples," *PHI Learning Pvt. Ltd*; 2012 Nov 18.

[8] F. Kholardi, M. Assili, M. A. Lasemi, and A. Hajizadeh, "Optimal management of energy hub with considering hydrogen network," In 2018 *International Conference on Smart Energy Systems and Technologies (SEST)*, 10-12 Sep 2018, pp. 1-6, IEEE. https://doi.org/10.1109/SEST.2018.8495664.

[9] J. Xu, F. Wang, C. Lv, Q. Huang, and H. Xie, "Economic-environmental equilibrium based optimal scheduling strategy towards wind-solar-thermal power generation system under limited resources," *Applied Energy*, vol. 231, pp. 355-71, 2018, https://doi.org/10.1016/j.apenergy.2018.09.113.

[10] A.E. Nezhad, M.S. Javadi, and E. Rahimi, "Applying augmented ε-constraint approach and lexicographic optimization to solve multi-objective hydrothermal generation scheduling considering the impacts of pumped-storage units," *International Journal of Electrical Power and Energy Systems*, vol. 55, pp. 195-204, 2014, https://doi.org/10.1016/j.ijepes.2013.09.006.

[11] S. A. Bukhari, W. Cao, X. Chen, F. Jandan, and D. Goswami, "Hybrid electric energy storage and its dynamic performance," *Cases on Green Energy and Sustainable Development 2020* (pp. 406-437). IGI Global.

[12] N. A. Khan, A. B. Awan, A. Mahmood, I. E. Member, S. Razzaq, A. Zafar, and G. A. Sidhu, "Combined emission economic dispatch of power system including solar photo voltaic generation," *Energy Conversion and management*; vol. 92, pp. 82-91, 2015, https://doi.org/10.1016/j.enconman.2014.12.029.

[13] Y. Zhu, J. Wang, and B. Qu, "Multi-objective economic emission dispatch considering wind power using evolutionary algorithm based on decomposition," *International Journal of Electrical Power & Energy Systems*; vol. 63, pp. 434-45, 2014, https://doi.org/10.1016/j.ijepes.2014.06.027.

[14] M. S. Fakhar, S. Liaquat, S. A. Kashif, A .Rasool, M. Khizer, M. A. Iqbal, M. A. Baig, and S. Padmanaban, "Conventional and metaheuristic optimization algorithms for solving short term hydrothermal scheduling problem: A review," *IEEE Access*; vol. 9, pp. 25993-6025, 2021, https://doi.org/10.1109/ACCESS.2021.3055292

[15] P. P. Biswas, P. N. Suganthan, and G. A. Amaratunga, "Optimal power flow solutions incorporating stochastic wind and solar power," *Energy Conversion and Management*, vol. 148, pp. 1194-207, 2017, https://doi.org/10.1016/j.enconman.2017.06.071.

[16] M. Dahmani, M. Fellah, N. Hezil, M.C. Benoudia, M. Abdul Samad, A. Alburaikan, H. Abd El-Wahed khalifa, and A. Obrosov, "Structural and mechanical evaluation of a new Ti-Nb-Mo alloy produced by high-energy ball milling with variable milling time for biomedical applications," *The International Journal of Advanced Manufacturing Technology*, vol. 129, no. 11, pp. 4971-91, 2023, https://doi.org/10.1007/s00170-023-12650-0.

[17] R. M. Zulqarnain, W. X. Ma, I. Siddique, A. Alburaikan, H. Abd El-Wahed Khalifa, and A. M. Alanzi, "Prioritization of thermal energy storage techniques using TOPSIS method based on correlation coefficient for interval-valued intuitionistic fuzzy hypersoft set," *Symmetry*, vol. 15, no. 3, pp. 615, 2023, https://doi.org/10.3390/sym15030615.

[18] A. Ullah, R. A. ZeinEldin, and H. A. Khalifa, "Investigation of the three-dimensional hybrid casson nanofluid flow: a cattaneo–christov theory," *ACS omega*, vol. 8, no. 12, pp. 10991-1002, 2023, https://doi.org/10.1021/acsomega.2c07750.

[19] M. Basu, "Multiobjective generation scheduling of fixed head hydrothermal power systems through an interactive fuzzy satisfying method and evolutionary programming technique," *Electric Power Components and Systems*, vol. 32, no. 12, pp. 1287-99, 2004, https://doi.org/10.1080/15325000490446764.

[20] M. Clerc, and J. Kennedy, "The particle swarm-explosion, stability, and convergence in a multidimensional complex space," *IEEE transactions on Evolutionary Computation*, vol. 6, no. 1, pp. 58-73, 2002, https://doi.org/10.1109/4235.985692.

[21] N. Yang, Z. Dong, L. Wu, L. Zhang, X. Shen, D. Chen, B. Zhu, and Y. Liu, "A comprehensive review of security-constrained unit commitment," *Journal of Modern Power Systems and Clean Energy*, vol. 10, no. 3, pp. 562-76, 2021, https://doi.org/10.35833/MPCE.2021.000255.

[22] I. Abdou, and M. Tkiouat, "Unit Commitment Problem in Electrical Power System: A Literature Review," *International Journal of Electrical & Computer Engineering*, vol. 8, no. 3, pp. 2088-8708, 2018, https://doi.org/10.11591/ijece.v8i3.pp1357-1372.

[23] W. Van Ackooij, I. Danti Lopez, A. Frangioni, F. Lacalandra, and M. Tahanan, "Large-scale unit commitment under uncertainty: an updated literature survey," *Annals of Operations Research*, vol. 271, no. 1, pp. 11-85, 2018, https://doi.org/10.1007/s10479-018-3003-z.

[24] R. Swain, and U. C. Mishra, "To the Chief Editor, Electric Power System Researchshort-Term Hydrothermal Scheduling Using Grey Wolf Optimization Algorithm," *Electric Power System Researchshort-Term Hydrothermal Scheduling Using Grey Wolf Optimization Algorithm*, https://dx.doi.org/10.2139/ssrn.4468244.

[25] V. K. Kamboj, A. Nandi, A. Bhadoria, and S. Sehgal, "An intensify Harris Hawks optimizer for numerical and engineering optimization problems," *Applied Soft Computing*, vol. 89, pp. 106018, 2020, https://doi.org/10.1016/j.asoc.2019.106018.

[26] I. G. Damousis, A. G. Bakirtzis, and P. S. Dokopoulos, "A solution to the unit-commitment problem using integer-coded genetic algorithm," *IEEE Transactions on Power Systems*, vol. 19, no. 2, pp. 1165-72, 2004, https://doi.org/10.1109/TPWRS.2003.821625.

[27] B. K. Das, R. Hassan, M. S. Tushar, F. Zaman, M. Hasan, and P. Das, "Techno-economic and environmental assessment of a hybrid renewable energy system using multi-objective genetic algorithm: A case study for remote Island in Bangladesh," *Energy Conversion and Management*, vol. 230, pp. 113823, 2021, https://doi.org/10.1016/j.enconman.2020.113823.

[28] L. Xie, P. M. Carvalho, L. A. Ferreira, J. Liu, B. H. Krogh, N. Popli, and M. D. Ilić, "Wind integration in power systems: Operational challenges and possible solutions," *Proceedings of the IEEE*, vol. 99, no. 1, pp. 214-32, 2010, https://doi.org/10.1109/JPROC.2010.2070051.

[29] N. Muralikrishnan, L. Jebaraj, and C. C. Rajan, "A comprehensive review on evolutionary optimization techniques applied for unit commitment problem," *IEEE Access*, vol. 8, pp. 132980-3014, 2020, https://doi.org/10.1109/ACCESS.2020.3010275.

[30] C. P. Cheng, C. W. Liu, and C. C. Liu, "Unit commitment by Lagrangian relaxation and genetic algorithms," *IEEE transactions on power systems*, vol. 15, no. 2, pp. 707-14, 2000, https://doi.org/10.1109/59.867163.

[31] L. Richter, M. Lehna, S. Marchand, C. Scholz, A. Dreher, S. Klaiber, and S. Lenk, "Artificial intelligence for electricity supply chain automation," *Renewable and Sustainable Energy Reviews*, vol. 163, pp. 112459, 2022, https://doi.org/10.1016/j.rser.2022.112459.

[32] H. Mori, and O. Matsuzaki, "Application of priority-list-embedded tabu search to unit commitment in power systems," *IEEE Transactions on Power and Energy*; vol. 121, no. 4, pp. 535-41, 2001.

[33] T. O. Ting, M. V. Rao, and C. K. Loo, "A novel approach for unit commitment problem via an effective hybrid particle swarm optimization," *IEEE Transactions on Power Systems*, vol. 21, no. 1, pp. 411-8, 2006, https://doi.org/10.1109/TPWRS.2005.860907.

[34] A. Y. Saber, T. Senjyu, N. Urasaki, and T. Funabashi, "Unit commitment computation-A novel fuzzy adaptive particle swarm optimization approach," *IEEE Power Systems Conference and Exposition*, pp. 1820-1828, 2006, https://doi.org/10.1109/PSCE.2006.296189.

[35] P. Sriyanyong, and Y. H. Song, "Unit commitment using particle swarm optimization combined with Lagrange relaxation," *IEEE Power Engineering Society General Meeting*, pp. 2752-2759, 2005, https://doi.org/10.1109/PES.2005.1489390.

[36] Z.L. Gaing, "Discrete particle swarm optimization algorithm for unit commitment," *IEEE Power Engineering Society General Meeting*, vol. 1, pp. 418-424, 2003, https://doi.org/10.1109/PES.2003.1267212.

[37] A. H. Mantawy, "A genetic algorithm solution to a new fuzzy unit commitment model," *Electric power systems research*, vol. 72, no. 2, pp. 171-8, 2004, https://doi.org/10.1016/j.epsr.2004.04.003.

[38] M. M. El-Saadawi, M. A. Tantawi, and E. Tawfik, "A fuzzy optimization-based approach to large scale thermal unit commitment," *Electric Power Systems Research*, vol. 72, no. 3, pp. 245-52, 2004, https://doi.org/10.1016/j.epsr.2004.04.009.

[39] P. Arévalo, M. Tostado-Véliz, and F. Jurado, "A novel methodology for comprehensive planning of battery storage systems," *Journal of Energy Storage*, vol. 37, pp. 102456, 2021, https://doi.org/10.1016/j.est.2021.102456.

[40] N. P. Padhy, "Unit commitment using hybrid models: a comparative study for dynamic programming, expert system, fuzzy system and genetic algorithms," *International Journal of Electrical Power & Energy Systems*, vol. 23, no. 8, pp. 827-36, 2001, https://doi.org/10.1016/S0142-0615(00)00090-9.

[41] T. T. Nguyen, D. N. Vo, B. H. Dinh, "An effectively adaptive selective cuckoo search algorithm for solving three complicated short-term hydrothermal scheduling problems," *Energy*, vol. 155, pp. 930-56, 2018, https://doi.org/10.1016/j.energy.2018.05.037.

[42] J. Jian, S. Pan, and L. Yang, "Solution for short-term hydrothermal scheduling with a logarithmic size mixed-integer linear programming formulation," *Energy*, vol. 171, pp. 770-84, 2019, https://doi.org/10.1016/j.energy.2019.01.038.

[43] H. Yin, F. Wu, X. Meng, Y. Lin, J. Fan, and A. Meng, "Crisscross optimization based short-term hydrothermal generation scheduling with cascaded reservoirs," *Energy*, vol. 203, pp. 117822, 2020, https://doi.org/10.1016/j.energy.2020.117822.

[44] R. S. Patwal, N. Narang, and H. Garg, "A novel TVAC-PSO based mutation strategies algorithm for generation scheduling of pumped storage hydrothermal system incorporating solar units," *Energy*, vol. 142, pp. 822-37, 2018, https://doi.org/10.1016/j.energy.2017.10.052.

[45] M. Kaur, J. S. Dhillon, and D. P. Kothar, "Crisscross differential evolution algorithm for constrained hydrothermal scheduling," *Applied Soft Computing*, vol. 93, pp. 106393, 2020, https://doi.org/10.1016/j.asoc.2020.106393.

[46] N. Narang, "Short-term hydrothermal generation scheduling using improved predator influenced civilized swarm optimization technique," *Applied Soft Computing*, vol. 58, pp. 207-24, 2017, https://doi.org/10.1016/j.asoc.2017.04.065.

[47] S. Özyön, "Optimal short-term operation of pumped-storage power plants with differential evolution algorithm," *Energy*, vol. 194, pp. 116866, 2020, https://doi.org/10.1016/j.energy.2019.116866.

[48] P. H. Chen, "Pumped-storage scheduling using evolutionary particle swarm optimization," *IEEE Transactions on Energy Conversion*, vol. 23, no. 1, pp. 294-301, 2008, https://doi.org/10.1109/TEC.2007.914312.

[49] F. A. Hashim, and A. G. Hussien, "Snake Optimizer: A novel meta-heuristic optimization algorithm," *Knowledge-Based Systems*, vol. 242, pp. 108320, 2022, https://doi.org/10.1016/j.knosys.2022.108320.

[50] P. V. Klimov, J. Kelly, J. M. Martinis, and H. Neven, "The snake optimizer for learning quantum processor control parameters," *arXiv preprint arXiv:*2006.04594, 2020, https://doi.org/10.48550/arXiv.2006.04594

[51] R. A. Khurma, D. Albashish, M. Braik, A. Alzaqebah, A. Qasem, and O. Adwan, "An augmented Snake Optimizer for diseases and COVID-19 diagnosis," *Biomedical Signal Processing and Control*, vol. 84, pp. 104718, 2023, https://doi.org/10.1016/j.bspc.2023.104718.

[52] I. Al-Shourbaji, P. H. Kachare, S. Alshathri, S. Duraibi, B. Elnaim, and M. Abd Elaziz, "An efficient parallel reptile search algorithm and snake optimizer approach for feature selection," *Mathematics*, vol. 10, no. 13, pp. 2351, 2022, https://doi.org/10.3390/math10132351.

[53] M. Kumar, and J. S. Dhillon, "Hybrid artificial algae algorithm for economic load dispatch," *Applied Soft Computing*, vol. 71, pp. 89-109, 2018, https://doi.org/10.1016/j.asoc.2018.06.035.

[54] J. S. Dhaliwal, and J. S. Dhillon, "A synergy of binary differential evolution and binary local search optimizer to solve multi-objective profit-based unit commitment problem," *Applied Soft Computing*, vol. 107, pp. 107387, 2021,

[55] N. Narang, J. S. Dhillon, and D. P. Kothari, "Multi-objective fixed head hydrothermal scheduling using integrated predator-prey optimization and Powell search method," *Energy*, vol. 47, no. 1, pp. 237-52, 2012, https://doi.org/10.1016/j.energy.2012.09.004.

[56] M. Nemati, M. Braun, and S. Tenbohlen, "Optimization of unit commitment and economic dispatch in microgrids based on genetic algorithm and mixed integer linear programming," *Applied Energy*, vol. 210, pp. 944-63, 2018, https://doi.org/10.1016/j.apenergy.2017.07.007.

[57] A. Kumar, and J. S. Dhillon, "Emended Harris Hawk Optimizer for Mixed Energy Generation Scheduling Problem," *Electric Power Components and Systems*, vol. 52, no. 8, pp. 1235-1268, 2023, https://doi.org/10.1080/15325008.2023.2239224.

[58] J. A. Duffie, and W. A Beckma, "Solar engineering of thermal processes," *John Willey & Sons, New York*, 1980.

[59] V. B. Vommi, and R. Vemula, "A very optimistic method of minimization (VOMMI) for unconstrained problems," *Information Sciences*, vol. 454, pp. 255-74, 2018, https://doi.org/10.1016/j.ins.2018.04.046.

[60] W. G. Spendley, G. R. Hext, and F. R. Himsworth, "Sequential application of simplex designs in optimisation and evolutionary operation. Technometrics," vol. 4, no. 4, pp. 441-61, 1962, https://doi.org/10.1080/00401706.1962.10490033.

[61] S. Rahnamayan, H. R. Tizhoosh, and M. M. Salama, "Opposition-based differential evolution," *IEEE Transactions on Evolutionary computation*, vol. 12, no. 1, pp. 64-79, 2008, https://doi.org/10.1109/TEVC.2007.894200.

[62] Z. Seif, and M. B. Ahmadi, "An opposition-based algorithm for function optimization," *Engineering Applications of Artificial Intelligence*, vol. 37, pp. 293-306, 2015, https://doi.org/10.1016/j.engappai.2014.09.009.

[63] A. A. Heidari, S. Mirjalili, H. Faris, I. Aljarah, M. Mafarja, and H. Chen, "Harris hawks optimization: Algorithm and applications," *Future Generation Computer Systems*, vol. 97, pp. 849-72, 2019, https://doi.org/10.1016/j.future.2019.02.028.

[64] N. Narang, J. S. Dhillon, and D. P. Kothari, "Scheduling short-term hydrothermal generation using predator-prey optimization technique," *Applied Soft Computing*, vol. 21, pp. 298-308, 2014, https://doi.org/10.1016/j.asoc.2014.03.029.

[65] J. S. Dhillon, J. S. Dhillon, and D. P. Kothari, "Real coded genetic algorithm for stochastic hydrothermal generation scheduling," *Journal of Systems Science and Systems Engineering*, vol. 20, pp. 87-109, 2011, https://doi.org/10.1007/s11518-011-5158-x.